國立臺灣大學電機資訊學院電機電信電子產業研發碩士專班

碩士論文

Industrial Technology R&D Master Program in Electrical, Communication and Electronics Engineering

College of Electrical Engineering and Computer Science

National Taiwan University

Master Thesis

光伏效率之快速提升技術

Efficiency Boosting Approaches for Photovoltaic Technology

殷瑞

Enrique Encinas Pollos

指導教授:劉致為 博士

Advisor: Chee Wee Liu, Ph.D.

中華民國 九十八 年 一 月

January 2009

98
1


國立臺灣大學
教育學術・愛國愛人

Related Publication (相關論文發表)

1. C.-H. Lin, Y.-J. Yang, E. Encinas, W.-Y. Chen, **J.-J. Tsai**, and C.W. Liu, “Single crystalline film on glass for thin film solar cells,” *2nd International Conference on Surfaces,Coatings and Nanostructured Materials, 2007.*

誌　謝

The completion of this thesis would have been impossible without the support and inspiration of many people. Here I would like to present my humble acknowledgements to those who have accompanied me in this academical path.

First of all, I would like to express my gratitude to Professor Chee Wee Liu (劉致為) my advisor during more than two years in National Taiwan University, who has provided me with an optimum working environment, extensive knowledge and has brilliantly guided me through all the steps of my research.

I am deeply indebted to Ángel Álvarez, my professor at Universidad Politécnica de Madrid (UPM) for his immense trust and help in this process even before it started, without him no words would be written in the following pages. I must also mention Alberto Almendra and Blanca Lopez from UPM for their aid and patience.

National Taiwan University has proven to be a marvelous institution that during the last two years has provided me, not only with extensive knowledge but also support and help when economical, cultural and academical problems arose, especially through Elaine Lee and Prof. Chang, Hung-Chun.

I am thankful to Prof Huang, Kuan, Lin and Liu that in the midst of all their activity, accepted to be members of the evaluation committee.

The discussions and cooperation with all of my colleagues have contributed substantially to this work: Ping-Sheng Kuo; Yen-Chun Fu; Hung-Chang Sun; Wei-Shuo

Ho; Ai-Ching Chou; Jack Shen and Jyong-Fong Liao deserve to be thanked for their advice and their willingness to share their bright thoughts with me.

I would like to pay the most sincere tribute to Jing-Jeng Tsai (蔡俊哲) a marvelous friend who has gifted me with his immeasurable support, and has given me a great amount of culturally intense moments during my stay in Taiwan, guiding me into a better understanding of a beautiful and complex new society.

My family deserves a special mention for being an infinite source of confidence and reinforcement. My mother, Asun Pollos who has carried the burden of my education all my life has being an example of sincerity and generosity, my father Enrique Encinas, my brother David Encinas, my uncle Jesus Pollos and all the rest, this is dedicated to you.

Words prove to be insufficient to show my appreciation to those whose contribution though indirect has also been essential and tremendously inspiring: Alla Eglite, Jose Ramón Durán, Felipe Lozano, Cerise Phiv, Val Lee, Chii Huan Lin, Sebastian and Stefanie Flores, Antonio Garzón, Lucas Eznarriaga, Rocío López Andino, Alvaro Castro and many others.

Finally, I would like to thank everybody who was important to the successful realization of thesis, as well as expressing my apology that I could not mention personally one by one.

摘要

在本論文中，提出三種方法來改善矽晶圓太陽能電池效率：金氧半結構太陽電池、利用浸沒式電漿離子佈值技術鈍化修補太陽電池表面缺陷和施加外應力於太陽電池以增加載子遷移率。

在結構上，製作了Al/SiO2/ p-type與ITO/SiO2/ n-type 兩種不同金氧半結構太陽電池元件，相較於鋁電極來說，因為ITO電極材料的介面特性，缺陷數較多，並無得到較鋁電極佳的光電轉換效率，亦透過ISE模擬軟體理論分析金氧半結構太陽電池。

製程上，利用浸沒式電漿離子佈值技術，對太陽能電池表面做氫鈍化層保護，降低表面複合速率，藉以增加光電流，太陽電池的光電效率可增強約16%。表面複合速率對太陽能電池參數影響透過模擬軟體研究。

最後，將現今廣泛應用於邏輯電路元件的應變矽技術，施加於矽晶圓太陽能電池上，藉由模擬軟體(ISE)來模擬與研究，模擬結果顯示此應力將會減少半導體能隙並增加光吸收，同時增強載子的遷移率，效率提升大約1.5%。

Abstract

In the present document, three different initiatives taken on behalf of efficiency improvement of wafer based solar cells are presented. First, MIS Solar cells are theoretically analyzed and the outcome is verified by means of TCAD simulation software. Al/SiO2/ptype Si and ITO/SiO2/nType Si devices are constructed and tested obtaining negative results that discard the utilization of transparent conductive oxides as promising contact materials for MIS solar cells.

The influence of front surface recombination on solar cell behavior is examined and an improvement methodology for this parameter by means of PIII technology is derived. PIII acts as a passivation method that tends to decrease the surface defects and hence decreases the surface recombination velocity. Experimental results reflect an efficiency increase of 16%.

Finally the impact of mechanically induced strain on solar cells is studied and modeled by software means. Results reveal a reduction in the semiconductor bandgap and a modification of the carrier mobilities that are translated into a 1.5% efficiency augmentation.

Contents

Chapter 3 PIII Passivation for Solar Cells

Chapter 4 Strain Technology in Photovoltaics

Chapter 5 Summary and Future Work

List of Figures

List of Tables

Chapter 1

Introduction

1.1 Motivation

Photovoltaic production has rocketed at a 27% annual rate since the year 1980 till 2007. The reasons underlying this magnificent rise in the usage of solar cell technology for energy acquirement are well known. Photovoltaic energy is essentially unlimited, clean and silent. The maintenance costs derived from its utilization are extremely low and the prospects of economical viability are realizable.

Historically, silicon has achieved the main role in most of semiconductor manufacturing schemes, and as a consequence, silicon is also the main actor in the photovoltaic technology scene. Wafer based (also known as first generation) solar cells represent the leading technology approach adopted by the market, a situation that is expected to remain until alternative technologies (thin film) are mature enough (technologically and economically efficient) to take the initiative.

In this thesis efficiency boosting techniques for wafer solar cells are developed in order to both take steps towards the achievement of the desired 1$/Watt milestone and provide performance enhancement approaches that may benefit the emerging photovoltaic technologies.

1.2 Outline

In the present document, three different initiatives taken on behalf of efficiency improvement of wafer based solar cells are presented. Each approach is elaborated in a different chapter configuring this thesis as follows.

Chapter 2, MIS solar cells are theoretically and experimentally analyzed and methods of efficiency improvement based on front contact modification are explored.

Chapter 3, the influence of front surface recombination on solar cell behavior is examined and an improvement methodology for this parameter by means of PIII technology is derived.

Chapter 4, Solar cells under strain conditions is investigated. By means of theoretical and simulated models, efficiency alterations are predicted.

Chapter 2

MIS Solar Cells

2.1 Introduction

A metal insulator semiconductor structure can be utilized with photovoltaic purposes if the insulator layer is very thin (20 to 30 angstroms). The advantages of using MIS as solar cells as compared to P-N junction solar cells are centered in the ease of fabrication, no diffusion processes are necessary, the low usage of materials, and the reduced degradation of carrier lifetimes as a consequence of the inexistence of high temperature fabrication processes. Research involving the development of new contacts based on transparent conductive oxides has been extensive over past years, and hence new concepts could be applied to MIS photovoltaic technology in order to improve previous results obtained with this solar cell technology.

In this chapter a theoretical analysis of the characteristics of MIS devices under dark conditions and under illumination will be carried in order to clarify its working principles. Simulation software will provide additional support to the theoretical conclusions derived. Finally, experimental results obtained from different fabricated MIS solar cells will be exposed, analyzed and compared with simulated data and theoretical models.

2.2 Theoretical Examination of MIS Solar Cells

The structure that determines a conventional MIS Solar Cell is shown in Figure 2.1. From direct inspection of the elements that constitute this device we can essentially differentiate three main parts: the substrate, the insulating layer and the contacts. The substrate is located at the bottom of the structure. We have chosen Si as the semiconductor material and P type as doping, whereas these conditions are not necessary, other substrate materials and doping can be selected [1].

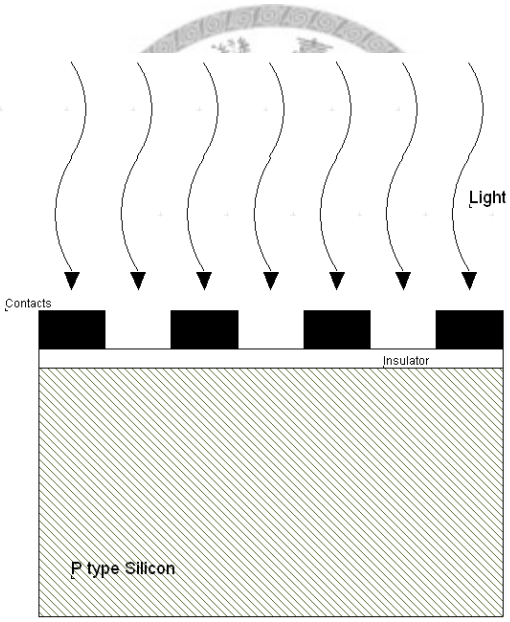

Figure 2.1 *Device structure of a conventional MIS Solar Cell*

On top of the substrate a very thin layer (usually less than 30 Angstroms) of insulating material, SiO2 in our case, is located. Metal-Semiconductor interfaces differ

from the expected behavior in that the electrostatic barriers formed are not as strongly dependent on the material work function as theoretical models predict. By inserting an insulating layer between the contacts and the substrate, the metal workfunction can dramatically affect the semiconductor, avoiding the non-ideality existing when no insulator is applied [2].

Finally, the top metal layer serves as both, a barrier inducer and a contact for the carriers to be collected. In order to facilitate the light penetration into the solar cell, very thin contacts can be utilized (less than 100A) and highly efficient grating lines can be engineered, so carriers are collected before recombining [3].

2.2.1 Dark current Analysis

The band diagram of a MIS diode at zero bias with P type Si substrate, SiO2 as an insulator and aluminum as a front contact in thermal equilibrium is shown in Figure 2.2. Ec stands for energy level of the conduction band, Ev is the energy level of the valence band, Ef and Ei are the Fermi level and the intrinsic Fermi level, , Φmi is the metal-insulator barrier that is related to Φm the metal workfunction , Φt is the difference between the Si and the SiO2 conduction band edges (3.2 eV) d is the insulator thickness, and Φb is the built in potential.

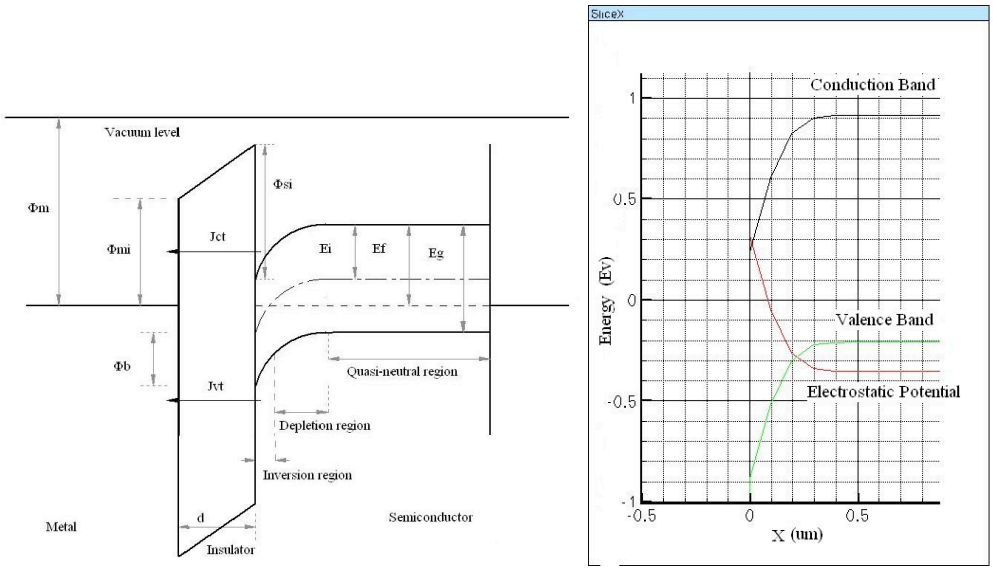

Figure 2.2 *MIS Diode Band Diagram under equilibrium*

In thermal equilibrium, Fermi levels must align, the Φm is chosen low in comparison with the Si Fermi level, so a potential drop occurs in the Si-Insulator interface as a consequence of the workfunction differences. This potential (Φb) is represented in Figure 2.2 as a band bending in Ec and Ev that creates an inversion layer and a depletion region in the semiconductor insulator surface. This region can be then used for electron-hole generation when the device is illuminated. The thickness of the insulator is chosen to be very thin in order to allow carriers to tunnel between metal and semiconductor. With this configuration the MIS diode becomes a minority carrier device with a very similar behavior to that of a p-n junction, the inversion layer being the n side of the junction and the Si substrate being the p side.

Hence, The IV characteristics of the Mis diode [4]:

$$I = I_s(e^{qV/nkT} - 1)$$

Being I_s the dark saturation current, q the charge, V the voltage applied, k the Boltzmann constant, T the temperature and n the ideality factor.

The current of the MIS diode without illumination [5]:

$$J = A^* T^2 e^{(-\alpha_t d\sqrt{q\Phi_t})} e^{\frac{-q\Phi_b}{kT}} \left[e^{qV/nkT} - 1\right]$$

Where A^* stands for the effective Richardson constant, Φb is the potential barrier and $e^{(-\alpha_t d\sqrt{q\Phi_t})}$ represents the tunneling probability for a rectangular barrier with an effective barrier height $q\Phi_t$ and width d.

This equation is very similar to the thermionic-emission equation that is applied for Schottky barrier devices with an additional tunneling term. When the insulator thickness decreases, or Φmi decreases, the current rapidly increases.

There are two main tunneling currents in the device: Jct (transport of carriers from the conduction band to the metal) and Jvt (transport of carriers from the valence band to the metal). In a MIS device with Al as metal and p type Si as a substrate, minority carrier (electron) Jct will be the dominant current component under reverse and small forward bias due to the abundance of electrons caused by the existence of an inversion layer [6].

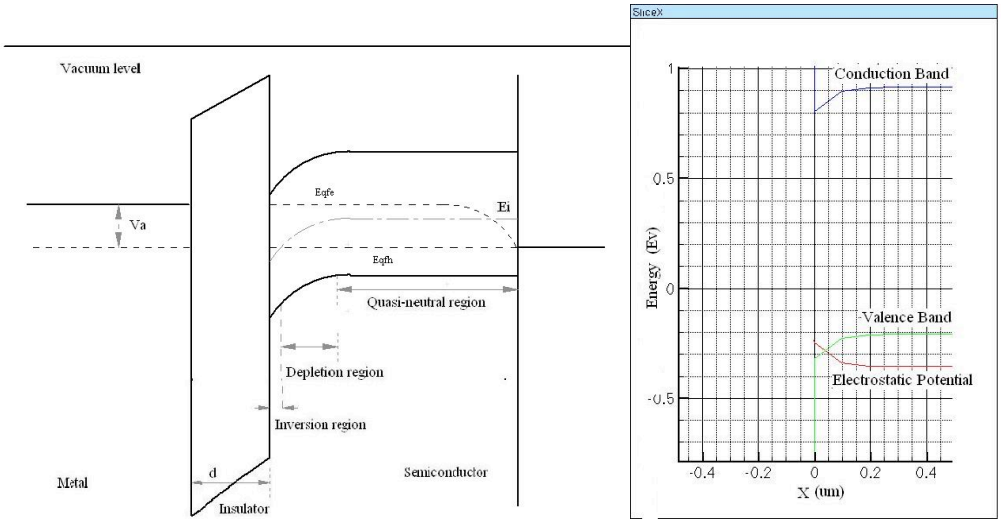

Figure 2.3 *Band Diagram of MIS Diode under small forward bias*

As the forward bias increases (applying positive voltage on the Si substrate), (Figures 2.3 and 2.4) the surface of the semiconductor goes from inversion to depletion and finally to accumulation, and the current increases monotonically.

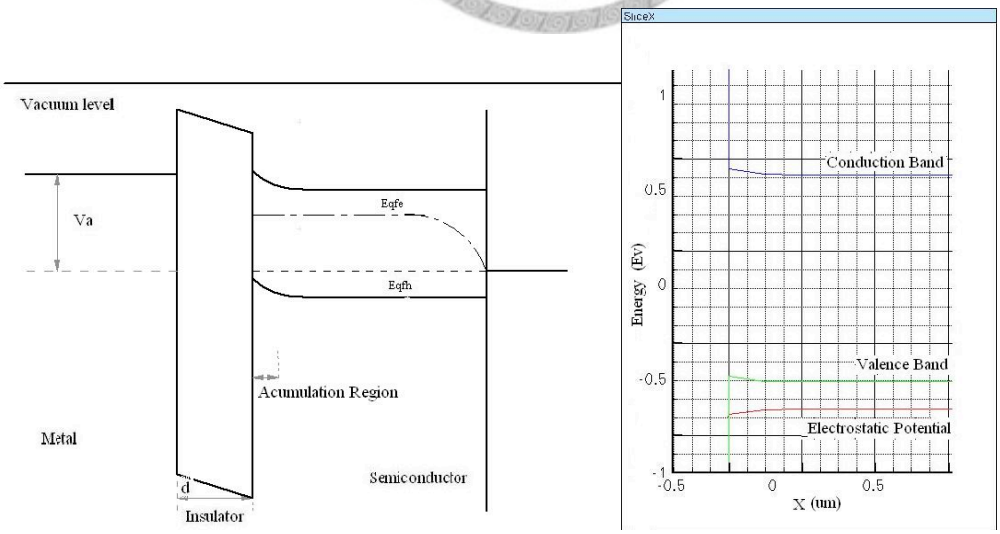

Figure 2.4 *Band Diagram of MIS Diode under moderate forward bias*

2.2.2 Illuminated Characteristics

As mentioned before, the MIS diode with p Si and Al as a metal contact behaves similarly to a p-n junction, as a consequence the total current under illumination [8]:

$$I = I_s(e^{qV/nkT} - 1) - I_l$$

The substrate region and the depletion region contribute with a component of photocurrent. From the Substrate region, considering the back contact is ohmic and the hole diffusion length is much smaller than the device thickness [9]:

$$J_n = qT(\lambda)\phi(\lambda)\frac{\alpha L_n}{\alpha L_n + 1}(e^{-\alpha W_D})$$

$T(\lambda)$ stands for the transmission coefficient of the metal $\phi(\lambda)$ is the number of photons per area per time per bandwidth and αL_n is the absorption coefficient multiplied by the electron's diffusion length.

In the Depletion region, the carriers are under the influence of a high electric field that enhances their collection by separating them before they can recombine. [10]:

$$J_{dr} = qT(\lambda)\phi(\lambda)(1 - e^{-\alpha W_D})$$

Total photocurrent will be the sum of both components:

$$J_L = J_n + J_{dr}$$

The Dark current as described in the previous section [11]:

$$J_s = A^{**}T^2 e^{(-\delta\sqrt{q\Phi_t})} e^{\frac{-q\Phi_b}{kT}}$$

Substitution I=0 in yields:

$$V_{oc} = \frac{nkT}{q}\left[\ln\left(\frac{J_L}{A^{**}T^2}\right)\right] + \frac{q\Phi_b}{kT} + \delta\sqrt{q\Phi_t}$$

This describes the behavior of Voc when a MIS diode is under illumination. By direct inspection this formula, a larger Φb will yield a higher value of Voc. The layer of insulating material in MIS devices pins the quasi electron Fermi level to the metal Fermi level under small forward biasing conditions, as a consequence, Φb increases. Increasing the insulator thickness will also increase Voc, but at the same time it will have a negative effect in the short circuit current, as carriers will find more difficulties to tunnel through the oxide. The optimum insulator thickness is found to be 2 nm.

2.2.3 Effect of Density of Interface Traps (DIT)

Interface states (traps) located in the semiconductor-insulator surface have the following properties: (1) They act as recombination centers where carriers recombine, (2) They are charge storage centers, (3) additional tunneling paths between semiconductor and metal can be established through them [12].

2.3 Simulation

In the following section, device simulations using ISE software are carried out in order to both verify the concepts explained in the theoretical analysis and calculate

the potential improvement that new materials could have in the development of MIS solar cells.

The main scope of this study is to analyze the influence that the material work function of the metal has on the device behavior.

2.3.1 Dark Current Analysis

The characteristics of the simulated device are defined as follows: P-type Si substrate with a doping of 1e16, 2nm thick layer of SiO2 and a metal with a workfunction that has been modified in order to analyze the IV curves and hence the influence of this parameter on the MIS device.

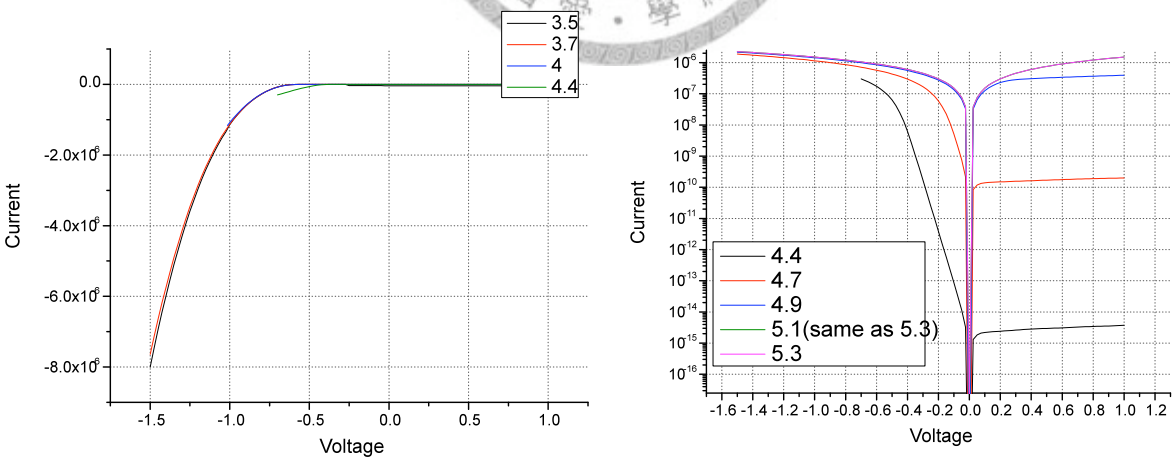

Figure 2.5 *Workfunction increase effect on P Silicon MIS structure*

When the oxide layer of the MIS device becomes very thin, tunneling currents affect the device, inducing a departure from thermal equilibrium conditions. In Figure 2.5 an increase of the dark current is observed when the metal workfunction is augmented, just as theoretical results predict. When the Om is larger, the band bending reduces, facilitating the tunneling of majority carriers (increase of Jvt).

For the case of a WF lower than 4.4 ev, the ratio of Jvt/Jct is very low, the device behaves as a minority carrier device and hence the current is reduced. The differences in the IV curves when the WF chosen are lower than 4.4 eV are not appreciated by the simulation program due to the low current values experienced by the device.

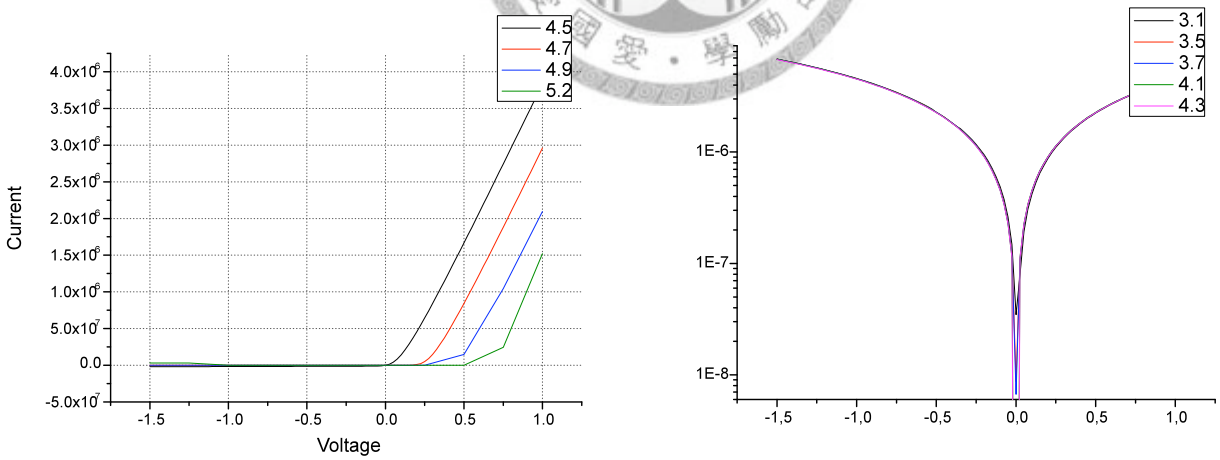

Figure 2.6 *Workfunction decrease effect on N type substrate MIS structure*

Figure 2.6 represent IV curves for N type Si substrate, it is observed that a

decrease in the metal workfunction affects the device, the same way an increase in the WF affected the P type substrate device.

2.3.2 DIT (Density of Interface Traps)

The following simulations explore the influence of the material workfunction and the DIT on the current-voltage behavior of the MIS diodes.

2.3.2.1. No Illumination

Traps are charge storage centers, a negative charge that is stored in the acceptor like states will decrease the band bending at the semiconductor/oxide interface [13]. This variation is traduced into a growth in Jvt (and decrease in Jct) and hence an increase in the net current. As Figure 2.7 shows, this variation of the band bending is mostly appreciated when the WF of the metal is low because it is in this case when Jpt is dominant. When the WF is increased, Jvt increases and eventually becomes dominant, so an additional increase due to traps is not noticeable (WF > 4.7)

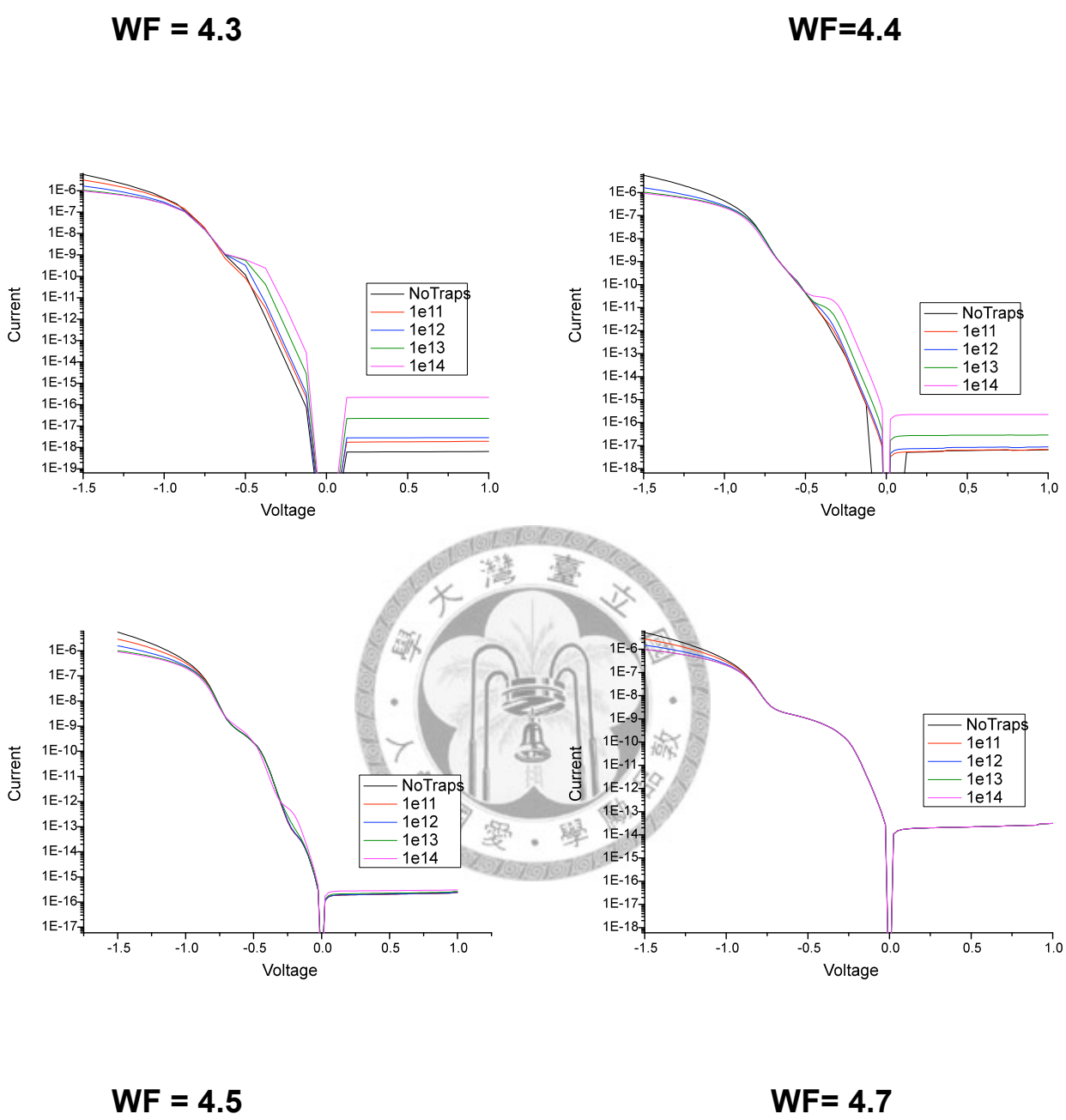

Figure 2.7 *Workfunction and Trap influence on MIS Diode under no Illumination*

2.3.2.2. Under illumination

The following figures represent IV curves of the device under study but when light is shown over the front surface of the device. The characteristics of the light source correspond with the A.M 1.5 spectrum.

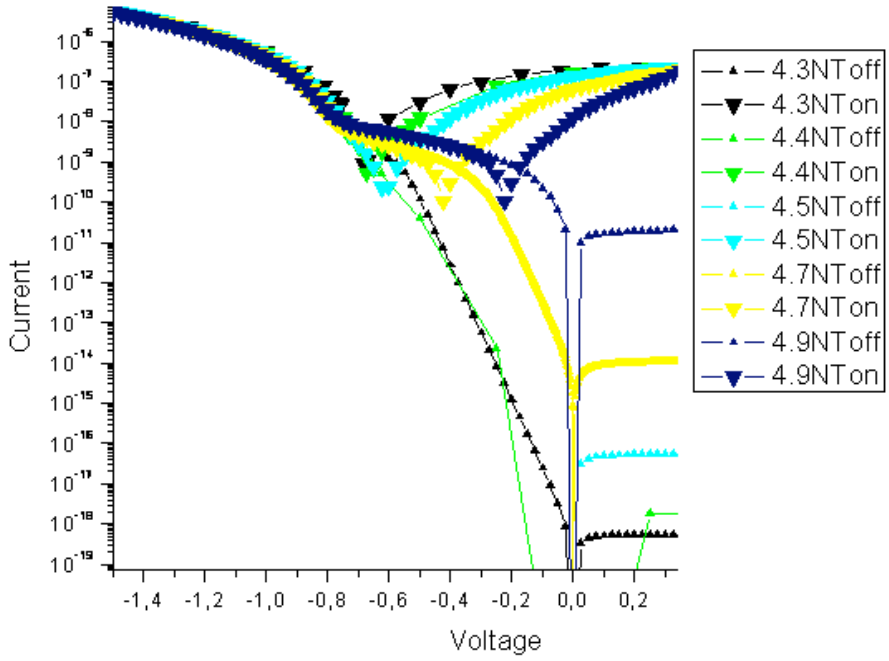

Figure 2.8 *Workfunction influence on MIS Diode under Illumination*

As we can observe from figure (right) a growth in the value of the workfunction represents a decrease of the Voc. This effect is attributed to the increase of the dark current as a consequence of the higher Om, an effect that has already being described in the previous section. At the same time Isc decreases because at higher

workfunction the width of the depletion region decreases.

When there are surface states, both Voc and Isc decrease (Figure 2.9). The first as a consequence of a higher dark current caused by the reduction of the band bending due to the fixed charges accumulated in the surface states. The latter decreases because surface states act as recombination centers, so photogenerated electron hole pairs recombine before they can contribute to the photocurrent.

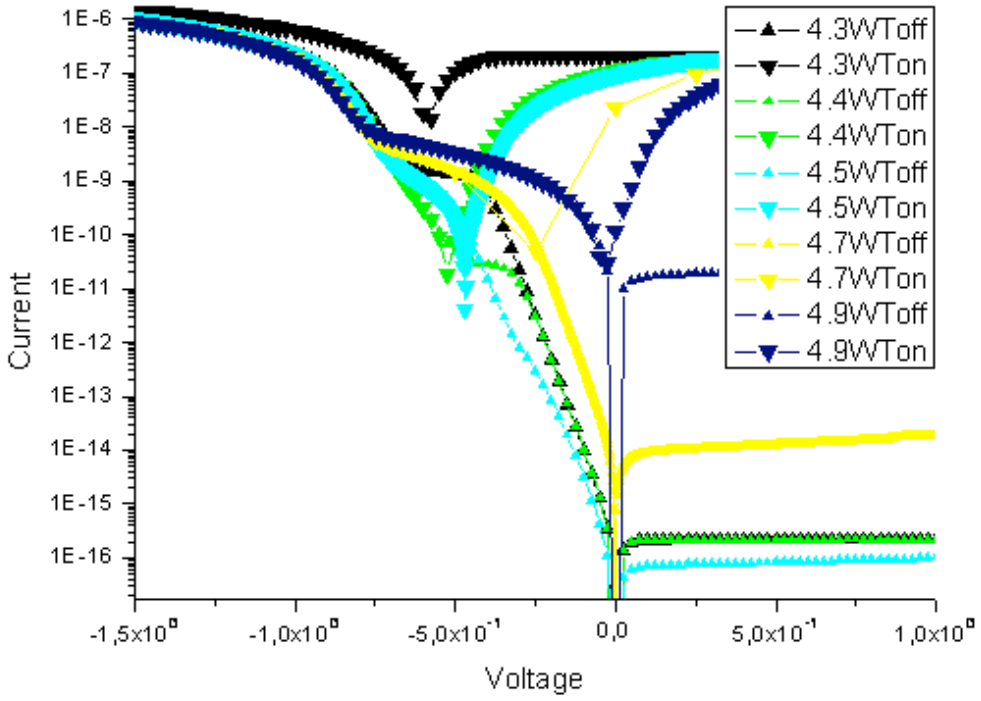

Figure 2.9 *Workfunction and Trap influence on MIS Diode under no Illumination*

Figure 2.10 shows the reduction of Voc and Isc as a function of the workfunction employed and the existence or non existence of surface states.

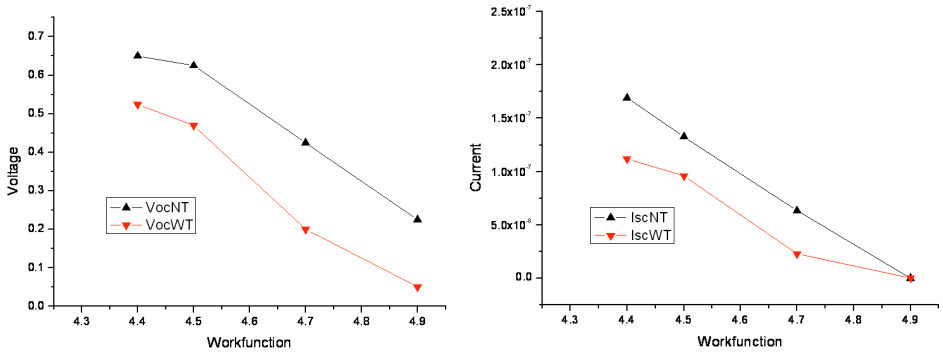

Figure 2.10 *Voc and Isc variation with Workfunction and Trap presence*

2.4 Experiments

2.4.1 Procedure

MIS solar cells with identical structure to that used in the simulation were built. Two different materials were used as contacts and both p type Si and n type si were used as substrate in order to evaluate the effect of a change of material workfunction in the solar cell behavior. Finally Aluminum/Sio2/ptypeSi, ITO/SiO2/ptypeSi, Aluminum/Sio2/ntypeSi and ITO/SiO2/ntypeSi solar cells were created.

P type boron and N type phosphorous doped silicon wafers with 1e16 as a doping density were used as a substrate.

The oxide layer existing in the device is grown by Liquid Phase Deposition

method. LPD with only H_2O addition is used, which was firstly attempted by Yoshitomi *et al.* [14] and studied by Yeh *et al.* [15]. In order to obtain a saturated solution with silica, silica (SiO_2) powder is added into hydrofluorosilicic acid (H_2SiF_6, 3.09 mol/l), maintaining the temperature constant at 30^oC, the solution is mixed with a magnetic stirrer, for 3 hours. Finally, the undissolved silica will be removed with filter paper. Addition of H_2O will enable the solution to become supersaturated with silicon acid.

Before deposition process, the native oxide on the substrates should be removed by introducing them in diluted HF solution for two minutes. After this step, the substrates are immersed in the silica saturated solution at 50^oC for 20 minutes.

After the deposition process, the samples are cleaned and dried with nitrogen gas. The oxide thicknesses obtained are measured by ellipsometer, and the values obtained are between 2~3nm.

Finally very thin, in order to allow illumination penetrate the device and create electron hole pairs, Aluminum contacts were evaporated (115 Angstrom thick) and ITO contacts were sputtered completing the MIS structure.

The formation of the back contact (ohmic contact) was completed by evaporating Aluminum with a thickness of 1000 Angstrom in every sample.

2.4.2 Results

The solar cells IV curves were measured using the Newport 150 W Oriel Solar

Simulator, as the light source and a IV tester. The results obtained will be analyzed in the following section.

2.4.2.1 Aluminum

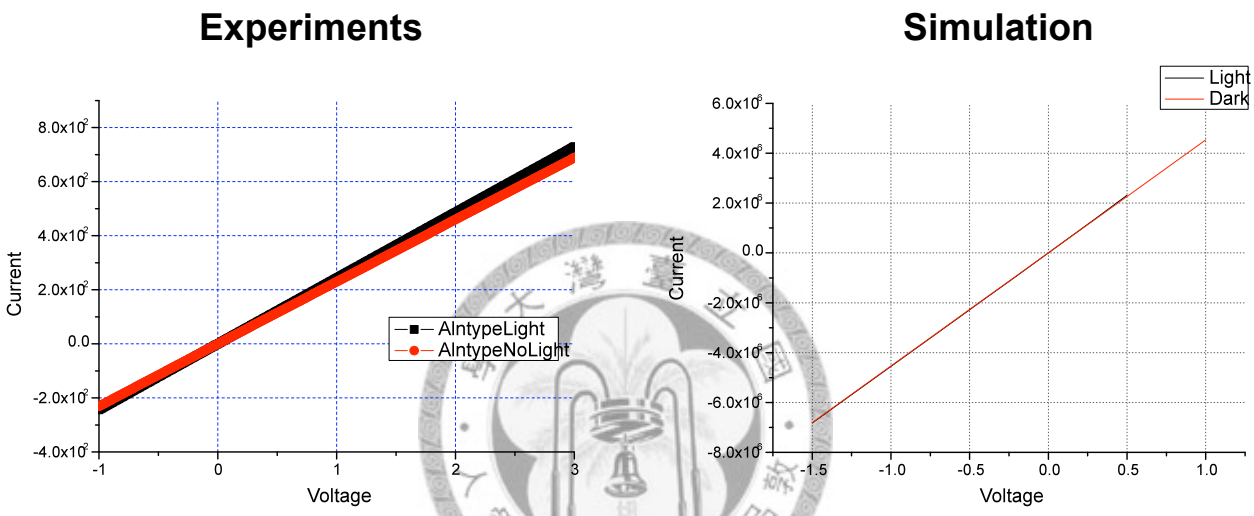

Figure 2.11 *IV characteristics of Al/SiO2/Ntype substrate cell*

The Figure 2.11 illustrates the Current-Voltage characteristics of the Al/SiO2/Ntype solar cell. As it was predicted by the theory there is no solar cell behavior in this MIS device when such a low workfunction metal is combined with an N type material.

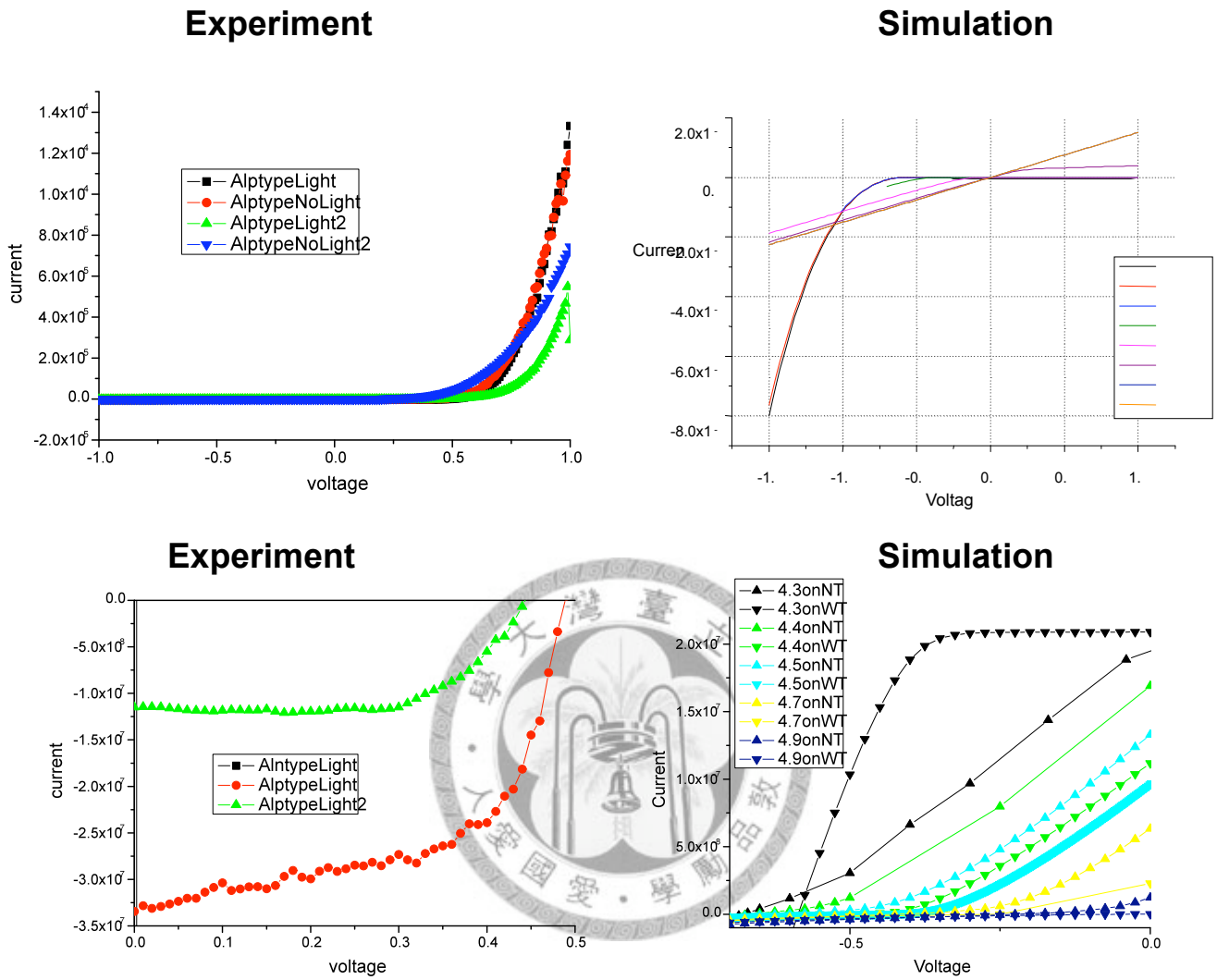

Figure 2.12 *Current-Voltage evaluation of Al/SiO2/ptype solar cell*

Figure 2.12 shows a comparison between the experiment and simulation results for the Al/SiO2/ptype solar cell. As we can see, the curves of the real and simulated device follow a similar qualitative tendency. The curve that corresponds with a WF of 4.3ev in the simulation resembles the curve of AlptypeLight (red) been mainly

differentiated by the absolute values of Voc and Isc.

2.4.2.2 ITO

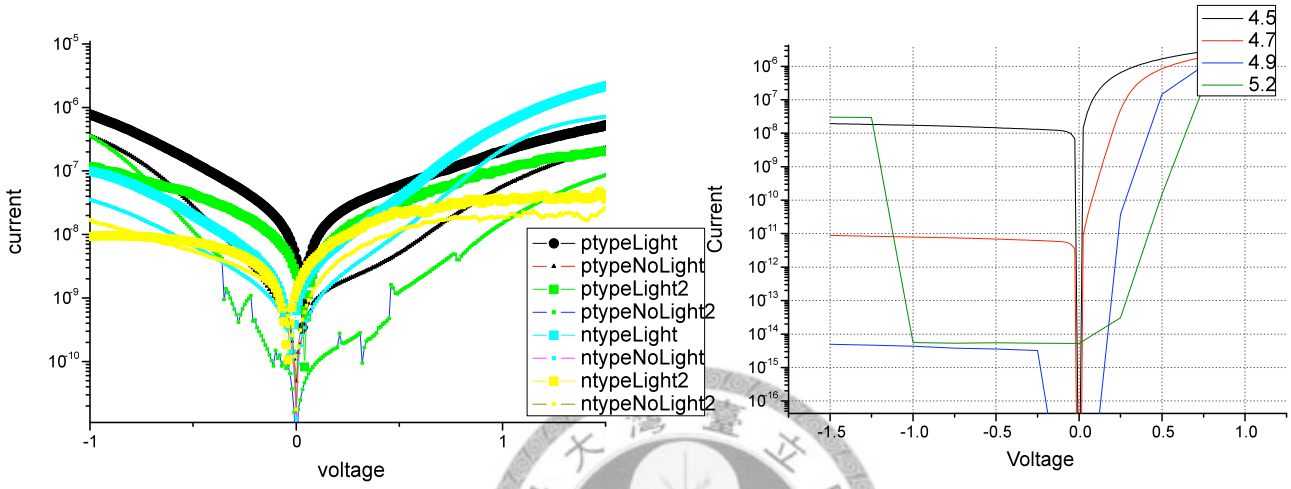

Figure 2.13 *ITO/SiO2/ptype & ITO/SiO2/ntype device analysis*

Simulated and experimental IV curves of the MIS solar cells with ITO as a front contact are shown in Figure 2.13. The behavior of the ITO/SiO2/ptype devices agrees with theoretical derivations as a high WF material is not suitable as a photovoltaic MIS device when combined with a p-type substrate. The experimental results for ITO/SiO2/ntype substrate under no illumination coincide with those simulated (ntypeNoLight experiments line with WF4.9 in the simulation) but the results obtained for the device under illumination appear to be very unfavorable, obtaining an Isc in the range of 10-8 and a Voc <0.1.

2.5 Discussion

The analysis of the experimental information obtained reveals results in agreement with the theoretical derivation from previous sections. A significant oscillation in the Isc value obtained between measurements carried on the same device points out the possibility of this experimental setup being not suitable for obtaining the required information. Extremely low values of Voc and Isc obtained with ITO/SiO2/nType can be attributed to the large amount of surface traps as a consequence of LPD oxide and also to the relatively poor conducting capabilities of ITO as compared to metals.

2.6 Summary

MIS devices were theoretically analyzed under dark current and illumination conditions. Simulations showed similar results to those theoretically predicted. MIS solar cells were fabricated, their IV curves obtained, and the results compared with those from simulated devices. Al/SiO2/ptype devices showed similar qualitatively results to those obtained from simulation while extremely negative results acquired with ITO/SiO2/nType substrate discard the utilization of transparent conductive oxides as promising contact materials for MIS solar cells.

References

[1] C.-H. Lin, Y.-J. Yang, E. Encinas, W.-Y. Chen, **J.-J. Tsai**, and C.W. Liu, "Single crystalline film on glass for thin film solar cells," *2nd International Conference on Surfaces,Coatings and Nanostructured Materials, 2007.*

[2] Martin A.Green, "Solar Cells Operating Principles, Technology and System Applications.",

[3] Martin A.Green, "Solar Cells Operating Principles, Technology and System Applications.",

[4] A. Luque, S. Hegedus, "Handbook of Photovoltaic Science and Engineering.", 2003,

[5] A. Luque, S. Hegedus, "Handbook of Photovoltaic Science and Engineering.", 2003, pag 440

[6] M.A.Green, F.D. King and J Shewchun "Minority carrier MIS tunnerl diodes and their application to electron and photovoltaic energy conversion – I Theory"

[7] A. Luque, S. Hegedus, "Handbook of Photovoltaic Science and Engineering.", 2003, pag 440

[8] A. Luque, S. Hegedus, "Handbook of Photovoltaic Science and Engineering.", 2003,

[9] A. Luque, S. Hegedus, "Handbook of Photovoltaic Science and Engineering.", 2003, pag 733

[10] A. Luque, S. Hegedus, "Handbook of Photovoltaic Science and Engineering.", 2003, pag 733

[11] A. Luque, S. Hegedus, “Handbook of Photovoltaic Science and Engineering.”, 2003, pag 734

[12] M.A.Green, F.D. King and J Shewchun “Minority carrier MIS tunnerl diodes and their application to electron and photovoltaic energy conversion – I Theory”

[13] Mohamed Yehya Doghish and Fat Duen Ho “A Comprehensive Analytical Model for Metal-Insulator-Semiconductor (MIS) Devices: A solar cell application” 1993

[14] S. Yoshitomi, S. Tomioka, and N. Haneji, ISDRS., p. 22, 1992.

[15] C. –F. Yeh, C. –L. Chen, and G. –H. Lin, J. Electrochem. Soc., 141, 3177 (1994).

Chapter 3

PIII passivation for Solar cells

3.1 Introduction

A major source of performance degradation in silicon solar cells is recombination, maintaining recombination levels very low greatly enhances the efficiency, especially at surfaces, where defects accumulate, it is crucial to passivate possible recombination centers in order to facilitate transport of carriers.

Plasma Immersion Ion Implantation (PIII) can be used to reduce the amount of surface defects and hence lower the recombination levels occurring at interfaces, by implantation of H ions, dangling bonds are passivated and hence the surface recombination velocity reduced.

In this chapter, a theoretical insight on the recombination mechanisms occurring at surfaces is obtained, simulated structures will be used to evaluate the impact of surface recombination velocity on solar cell performance and finally experiments are carried out in which commercial solar cells are PIII treated through different procedures. Finally, through and extensive study of all the obtained results, PIII passivating characteristics are examined and its possible application for solar cell efficiency enhancement evaluated.

3.2 Theoretical Considerations

3.2.1 Surface Recombination

Impurities and defects existing in semiconductors can give rise to allowed energy states within the forbidden bandgap of the material. These allowed energy states are very efficient recombination centers and as a consequence degrade the solar cell performance. The recombination process occurring in these impurities is presented in figure 3.1(Left)

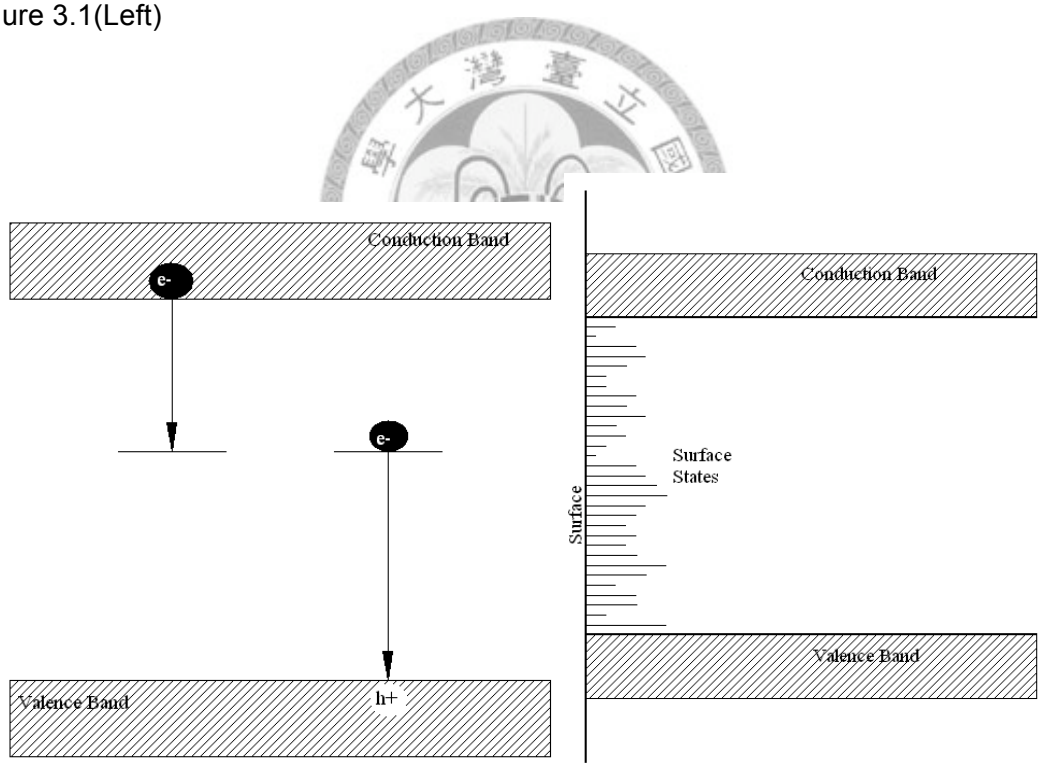

Figure 3.1 *Illustration of the two step recombination process (Left) and surface states (Right)*

This mechanism is known as two step recombination process. An electron from the conduction band relaxes to a defect risen allowed energy state located within the forbidden bandgap and afterwards relaxes to the valence band energy, annihilating a hole.

The net generation rate by traps can be expressed by [1]

$$U_t = \frac{np - n_i^2}{\tau_{h0}(n + n_1) + \tau_{e0}(p + p_1)}$$

n stands for the density of electrons in the conduction band, p is the density of holes in the valence band, τ_{h0} and τ_{e0} are the lifetime parameters depending on the type of trap and trap density and n_1 and p_1 can be expressed as [2]:

$$n_1 = N_c \exp\frac{E_t - E_c}{kT}$$

$$n_1 p_1 = n_i^2$$

This shows that there is a dependency between the net recombination rate and the defect energy level. If τ_{e0} and τ_{h0} are similar in magnitude, it is observed that impurities that introduce energy levels near the midgap are the most effective

recombination centers.

Surfaces represent significative disruptions in the crystal structure and are the site of many allowed energy states (figure2.1, right)

The expression for a single level surface state takes the form [3]

$$U_A = \frac{S_{e0}S_{h0}(np - n_i^2)}{S_{e0}(n + n_1) + S_{h0}(p + p_1)}$$

Where S_{e0} and S_{h0} are the surface recombination velocities for electrons and holes respectively. The conclusion of mid level traps being the most effective recombination centers is maintained as far as recombination at surfaces is concerned.

The current voltage characteristic of a solar cell takes the form as explained in the previous chapter:

$$I = I_s(e^{qV/nkT} - 1) - I_l$$

When a solar cell with finite dimensions is analyzed Figure 3.2, the expression that describes its dark saturation current (I_0) follows [4]

$$I_0 = A\left(\frac{qD_e n_i^2}{L_e N_A} * F_P + \frac{qD_h n_i^2}{L_h N_D} * F_N\right)$$

A being the area of the solar cell, q the charge D_e and D_h the electron and hole diffusion coefficients, L_e and L_h the electron and hole diffusion lengths, N_A and N_D the concentration of acceptor and donor impurities, n_i^2 the intrinsic concentration of carriers and finally F_P and F_N, terms that arise from considering the finite dimensions of a solar cell.

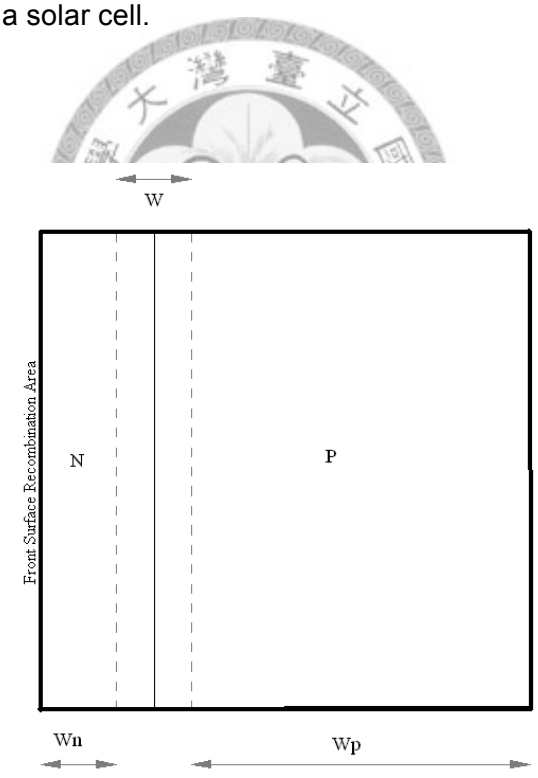

Figure 3.2 *Schematic of the solar cell considered for the theoretical analysis*

As far as we are mainly focusing on the front surface recombination,

$$F_N = \frac{S_h \cosh(W_N / L_N) + D_h / L_h \sinh(W_N / L_h)}{D_h / L_h \cosh(W_N / L_h) + S_h \sinh(W_N / L_h)}$$

Finally, a relation between the surface recombination velocity and the dark current can be established.

3.2.2 Influence on a solar cell's main parameters

The magnitude of surface recombination velocity (S_{rv}) will affect the parameters that describe the solar cell behavior: I_{sc} V_{oc} FF and η (efficiency).

An increase in the surface recombination velocity means that a larger amount of photo-generated electron hole pairs will recombine before reaching the contacts and contributing to the photocurrent. In other words, surface recombination velocity negatively affects the photo generated current and hence decreases I_{sc}.

As it has been shown in the previous section, higher values of the surface recombination velocity mean higher dark saturation currents. The expression that describes V_{oc} relates this parameter to the dark saturation current (I_0). [5]

$$V_{oc} = \frac{kT}{q}\ln(\frac{I_L}{I_0} + 1)$$

It then can be concluded that higher S_{rv} act to increase I_0 and hence decrease V_{oc}

The FF stands for [6]:

$$FF = \frac{V_{mp} I_{mp}}{V_{oc} I_{sc}}$$

Even though the previous expression relates I_{sc} and V_{oc} to the value of FF, a very accurate empirical expression relates the latter mainly to the magnitude of V_{oc} [7]:

$$FF = \frac{v_{oc} - \ln(v_{oc} + 0.72)}{v_{oc} + 1}$$
$$v_{oc} = V_{oc} / (kT/q)$$

From direct inspection of the previous formula, increasing S_{rv} will decrease V_{oc} and furthermore decrease the FF. The FF value relays on two parameters, Rs and Rsh, which are used to describe the real solar cell behavior. An increase in the Io can

be seen as a reduction in the Rsh [6]. Rs depends on the bulk resistance of the semiconductor, the bulk resistance of the contacts and the contact resistance between the contact and the semiconductor. Increasing Srv increases the latter term hence increasing Rs. The variation of FF when Rs is varied is observed in Figure 3.3 similar simulated results are obtained (Figure 3.4) when Srv is modified, a relation between Rs and Srv can then be established.

Higher Rs and lower Rsh both act reducing the FF.

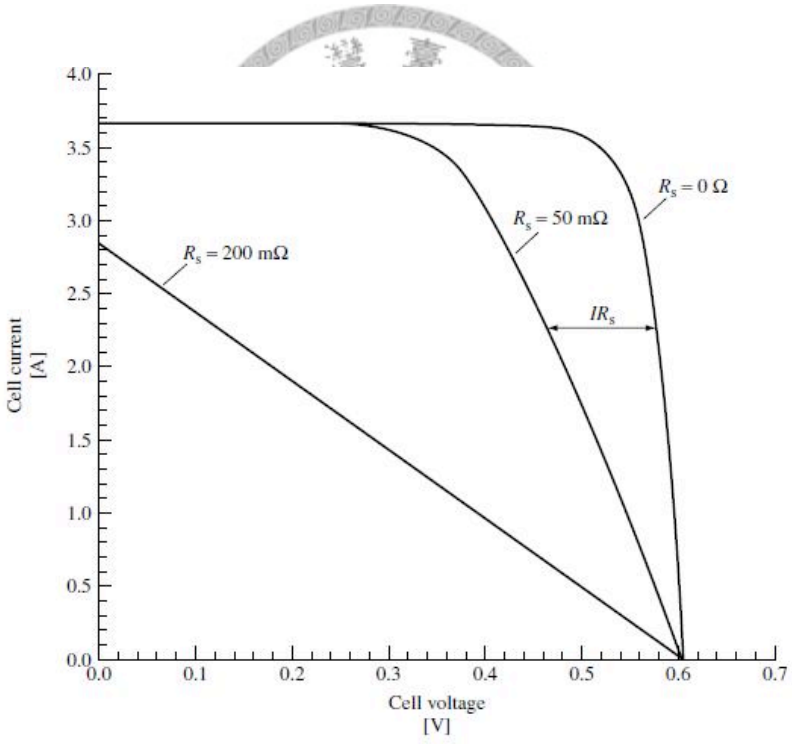

Figure 3.3 *Effect of series resistance on the current-voltage characteristics of a solar cell. Based on [4]*

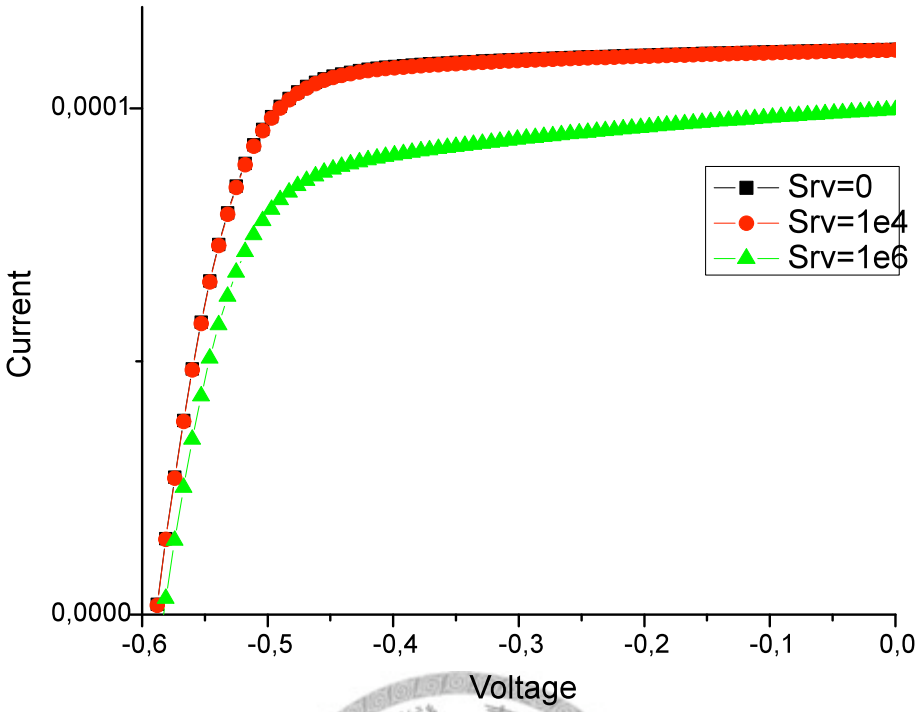

Figure 3.4 *Effect of surface recombination velocity on the current-voltage characteristics of a solar cell.*

The energy conversion efficiency of a solar cell is given by the expression[8] :

$$\eta = \frac{V_{mp} I_{mp}}{P_{in}} = \frac{V_{oc} I_{sc} FF}{P_{in}}$$

Larger values of S_{rv} act to decrease the value of I_{sc}, V_{oc} and FF, considering the influence of these parameters on η, and that the power incident on the device is constant, it is simply assured that η will decrease as well.

3.2.3 Plasma Immersion Ion Implantation (PIII)

Plasma Immersion Ion Implantation is an alternative technology to beamline ion implantation introduced in the semiconductor industry in the 1980's. The different processes that a PIII chamber is able to conduct are illustrated in Figure 3.5

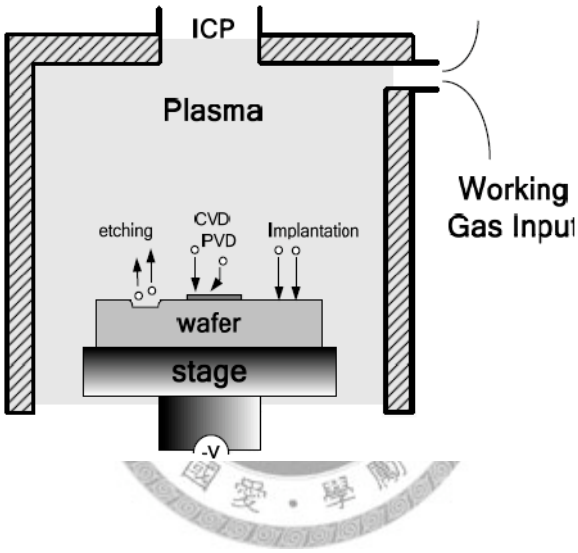

Figure 3.5 *Illustration of a PIII process chamber*

Hydrogenation of polysilicon flat panel displays [9], fabrication of thin oxide on SiGe [10], production of Silicon on insulator substrates [11][12], and shallow junction formation by plasma doping [13][14] are among the many applications of PIII technology in the semiconductor industry.

In this chapter experimental results on the hydrogen implantation by PIII on the

top surface of solar cells will be reported. It is expected that low energy hydrogen ion implantation acts to passivate defects and dangling bonds, decreasing the amount of surface states and as a consequence reducing the magnitude of the surface recombination velocity in the front surface of the solar cell.

3.3 Surface Recombination Velocity Simulation Results

Simulation results obtained from the simulation software ISE are presented in the following section. The magnitudes of I_{sc}, V_{oc}, FF and η versus different values of S_{rv} are plotted and analyzed.

3.3.1 Short Circuit Current (Isc)

The magnitude of Isc decreases when increasing Srv as it is observed in Figure 3.6. As far as the simulated solar cell dimensions are very small, the obtained values of Isc are also very small (10-4 10-5 A), so the influence of Srv is better appreciated in Figure 3.7, where the relative Isc variation percentage is plotted against Srv. A reduction of around 10.9% when Srv equals 1e6 with respect to no Srv is appreciated.

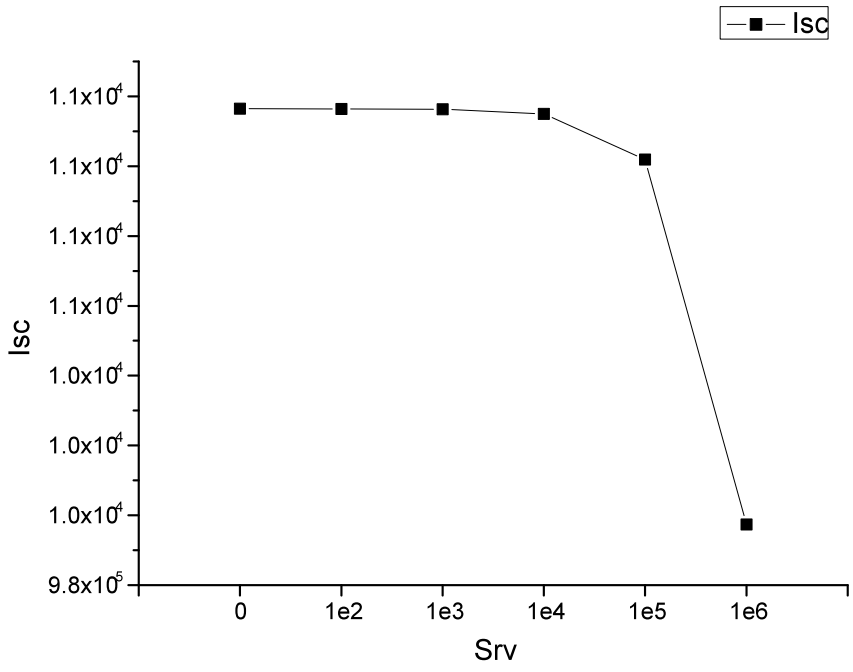

Figure 3.6 *Absolute variation of Isc against Srv*

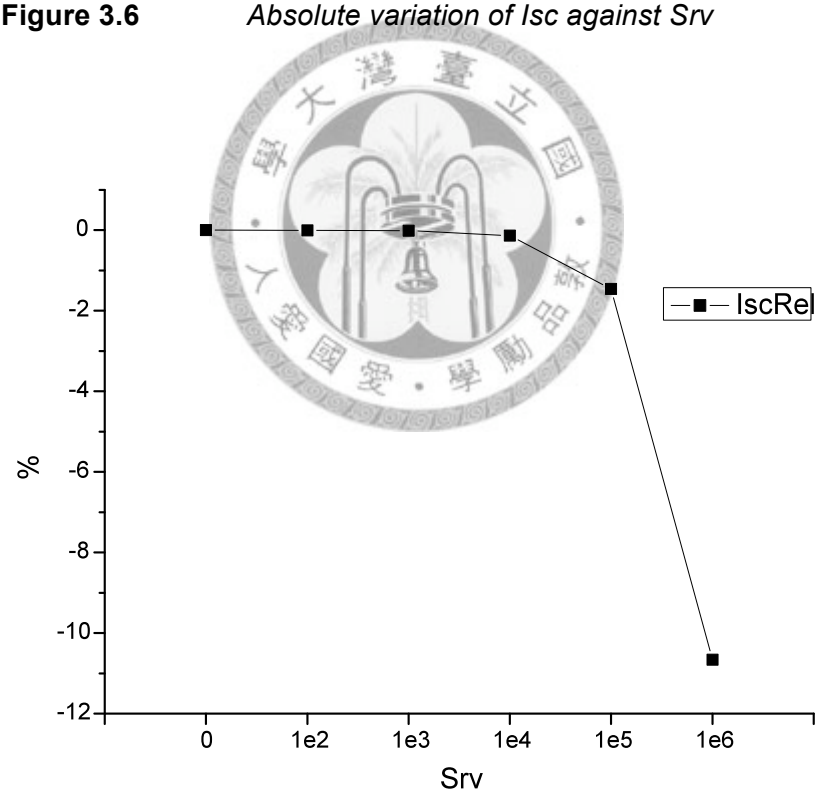

Figure 3.7 *Relative variation of Isc against Srv*

3.3.2 Open Circuit Voltage (Voc)

Voc follows a similar behavior with respect to Isc, but the influence of modifying Srv is not as significant. As we can observe in Figure 3.8, the impact on the Voc magnitude only represents a 1.6 % relative variation. The Voc is initially 0.594 V and descends to 0.584 V when Srv=1e6 Figure 3.9.

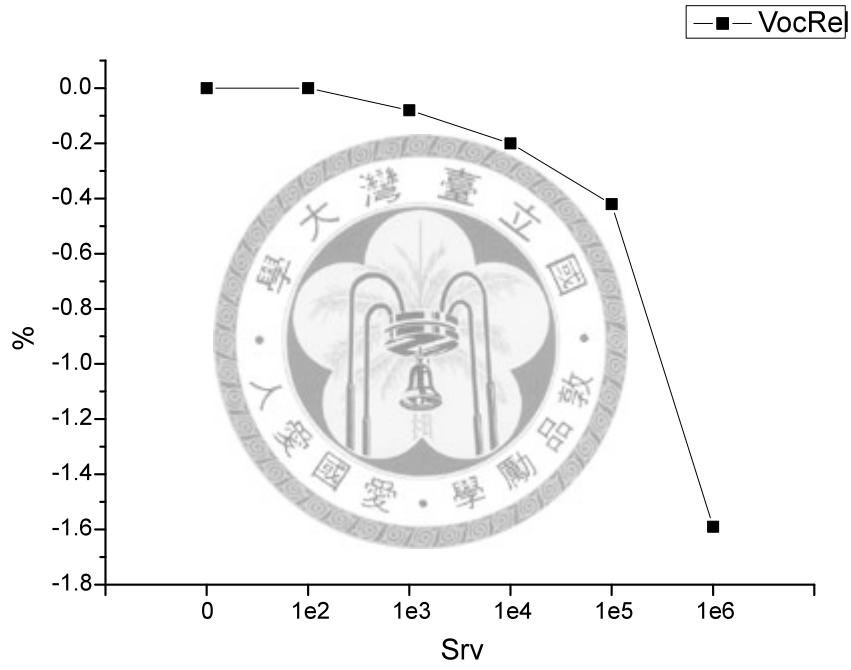

Figure 3.8 *Relative variation of Voc against Srv*

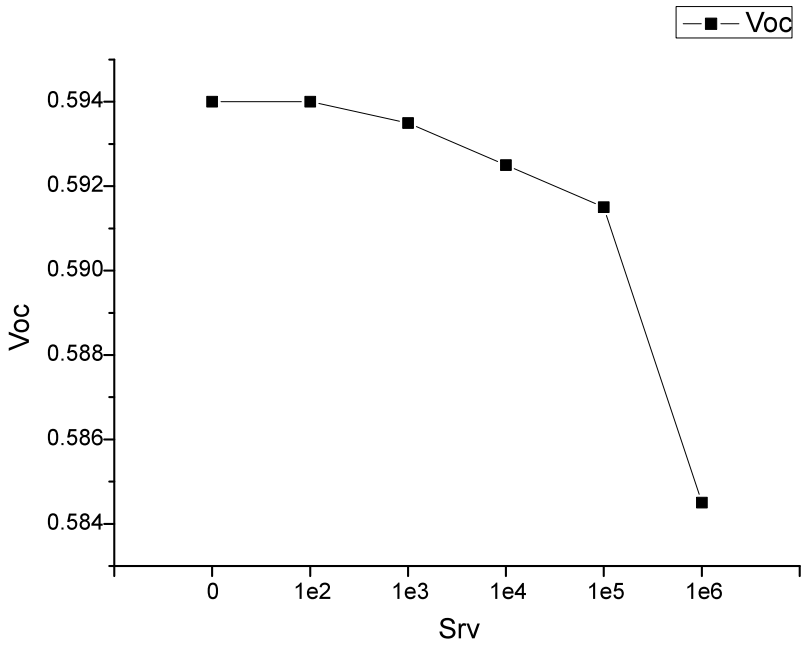

Figure 3.9 *Absolute variation of Voc against Srv*

3.3.3 Field Factor (FF)

FF decreases as well when the Srv is increased, FF varies from 74.3% to 68.6%.

Figure 3.10

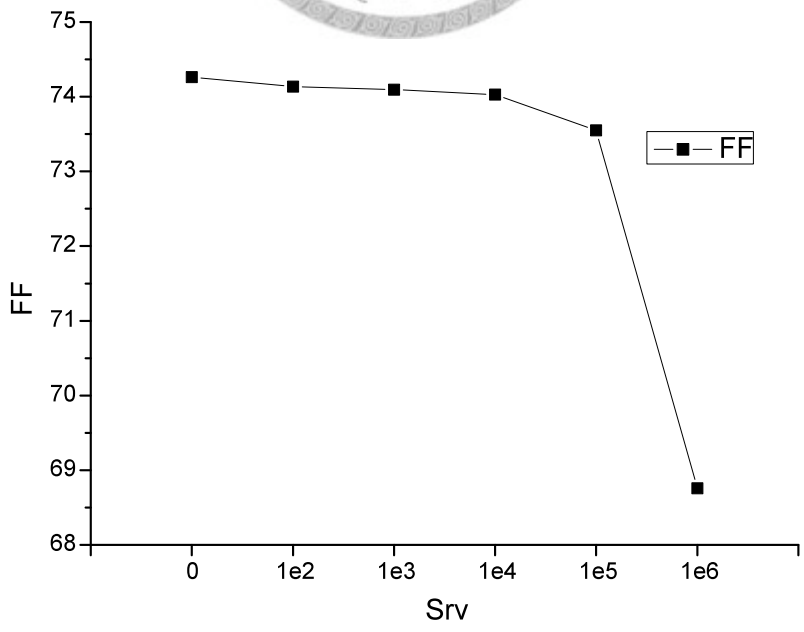

Figure 3.10 *Absolute variation of FF against Srv*

In this case the graph reflects a relative variation of 7.5 % from the initial Srv=0 value Figure 3.11

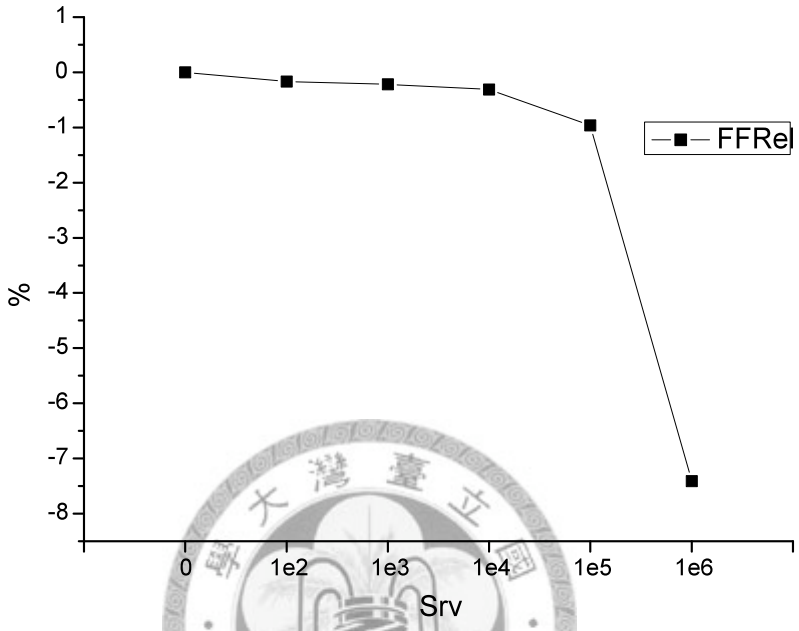

Figure 3.11 *Relative variation of FF against Srv*

3.3.4 Efficiency

Initially the efficiency accounted for a 10.03%, when Srv=1e6 there is a relative 18% efficiency reduction figure 2.9b. The final efficiency is 8.2% figure 2.9a

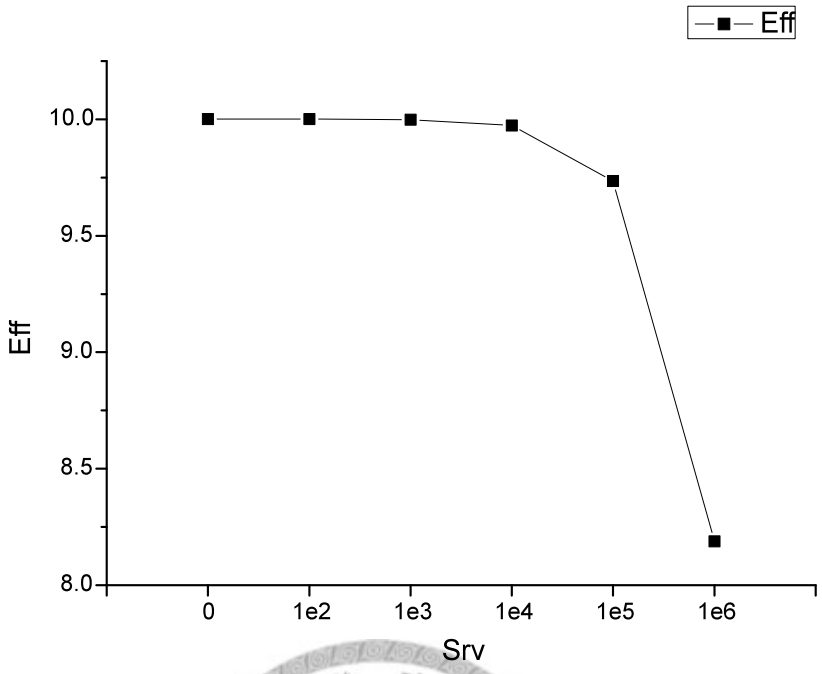

Figure 3.12 *Absolute variation of Eff against Srv*

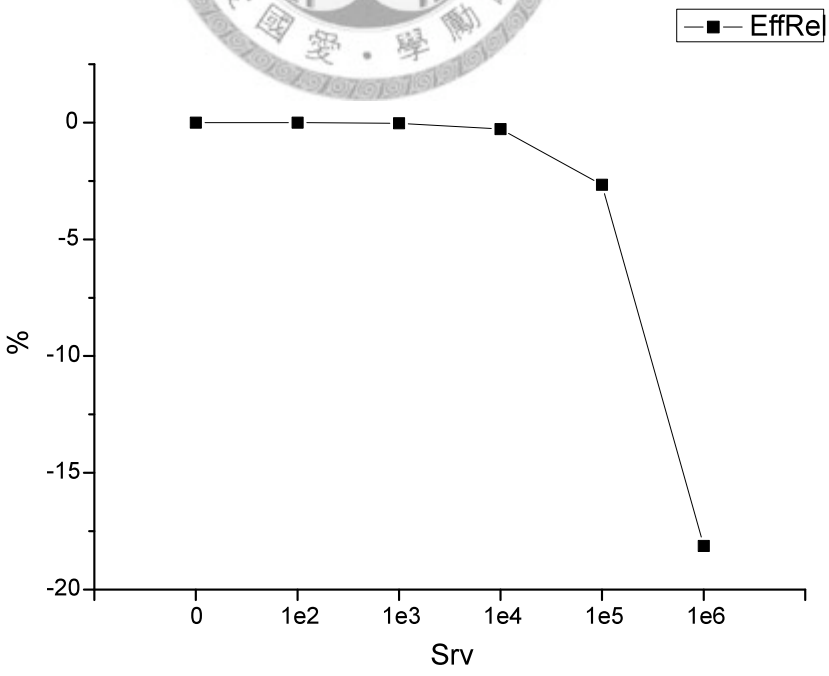

Figure 3.13 *Relative variation of Eff against Srv*

3.3.5 Conclusions

Simulation results follow a close relationship with respect to the theoretical analysis carried out in previous sections.

The greatest variation in all four parameters occurs in the Srv range 1e4 to 1e6, variation when Srv = 0 to 1e4 is not as significant as compared to the former range. A main reduction in Isc and FF is observed as compared to the variation experienced by the Voc.

The impact of photocarrier recombination and the increase of Rs are the physical mechanisms that have a stronger influence on the solar cell behavior when Srv varies.

3.4 Experiments

Solar cells have been passivated using PIII in order to reduce Srv on its top surface and hence improve its photovoltaic characteristics.

3.4.1 Procedure

6 inch Mono Crystalline Silicon solar cells purchased from Mosel Vitelic INC. were divided into 1 cm^2 fragments and two of them were labeled as sample2 and sample3 to carry out these experiments.

Sample2 and Sample3 IV characteristics under illumination were initially measured with the Solar Simulator Quicksun 120CA from Endeas using the two wire method, in order to obtain reference values for Isc, Voc, FF and efficiency. (Measurement configuration is illustrated in Figure 3.14)

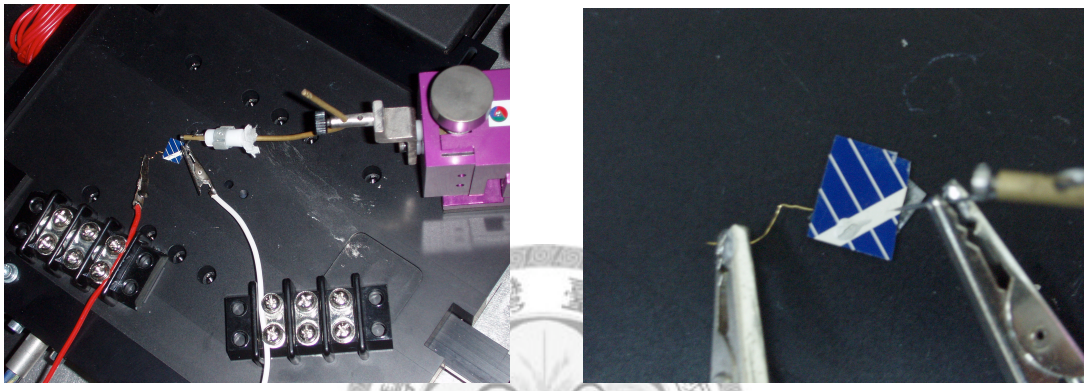

Figure 3.14 *PIII Experimental measurement configuration*

Sample2 was then PIII treated (detailed equipment used for this purpose is shown in Figure 3.15) for 60 seconds with an implant pulse voltage of 1kev. Sample3 was treated for 120 seconds also with an implant pulse voltage of 1Kev.

Finally Sample2 and Sample3 IV characteristics were measured following the method illustrated in Figure 3.14 and Isc, Voc, FF and efficiency extracted and compared to those initially obtained before PIII treatment was applied.

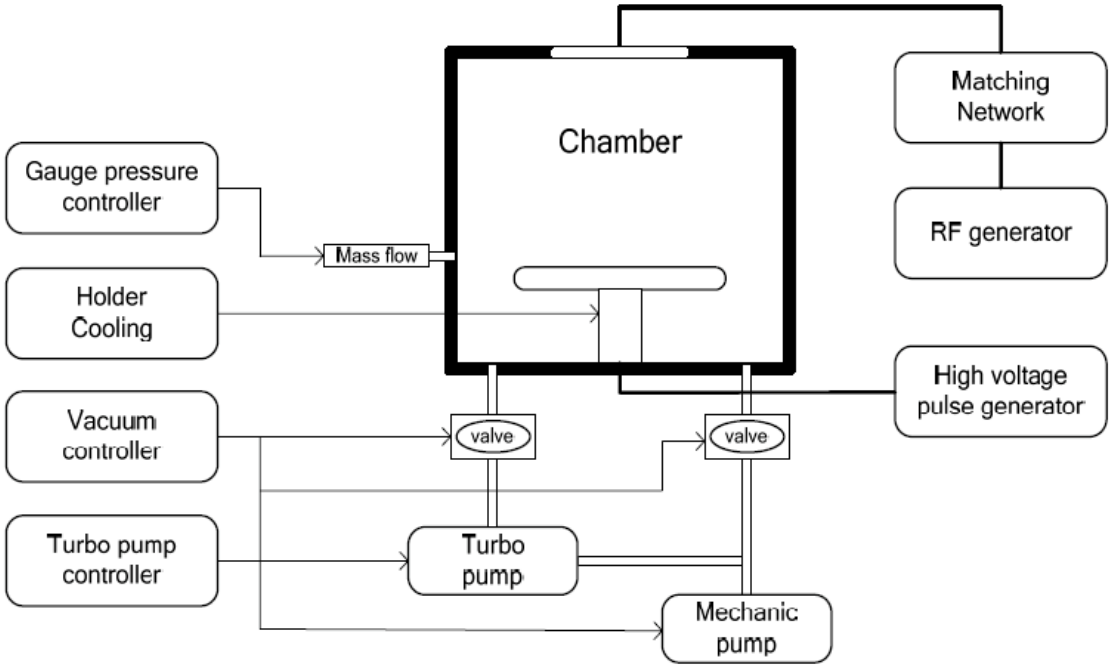

Figure 3.15 *PIII treatment equipment schematic*

3.4.2 Results

Table 3.1 and 3.2 reflect the impact PIII treatment has on the major solar cell parameters: Voc, Isc, FF and Eff.

Sample2-60s	Original	PIII
Isc	*19.48mA*	*24.33mA*
Voc	*0.5682 V*	*0.5772 V*
F.F	*0.695*	*0.658*
Efficiency	*9.2%*	*10.67%*

Table 3.1 *PIII impact on solar cell (sample 2) main parameters*

Sample3-120s	Original	PIII
Isc	*17.69mA*	*22.33mA*
Voc	*0.5794 V*	*0.5859 V*
F.F	*0.78*	*0.724*
Efficiency	*10.58%*	*12.43%*

Table 3.2 *PIII impact on solar cell (sample3) main parameters*

A better analysis on the effect PIII has on the solar cell can be carried out if Figure 3.16 is observed.

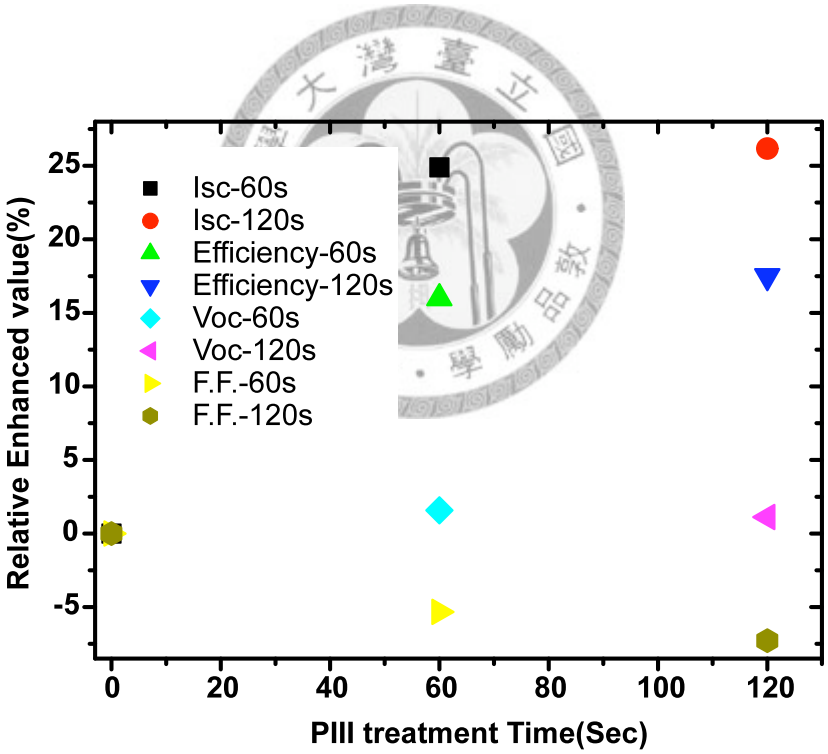

Figure 3.16 *Enhancement of main solar cell parameters vs. PIII treatment time*

It represents the relative variation of ISC, Voc, FF and Eff with respect to the PIII treatment time. Isc increases 24.22% after being treated for 60s and 26.8% after 120 seconds with respect to the untreated value. Voc experiences an increase of 1.5% and 1.1% after 60s and 120s treatment time respectively. The FF decreases when increasing PIII treatment time, 5.6% and 7.73% after 60s and 120s respectively. As a consequence of the variation of Isc Voc and FF, efficiency increases 15.97% after 60s treatment time and 17.48 after 120s.

3.5 Discussion

The results obtained in the previous section are in concordance with the theoretical derivations from section 3.2. PIII acts as a passivation method that tends to decrease the surface defects and hence decreases the surface recombination velocity.

Isc increases after PIII is applied in the surface because PIII reduces the surface defects and as a consequence the amount of carriers that recombine in the surface instead of contributing to the photocurrent is drastically reduced.

PIII acts to reduce the dark saturation current and hence the Voc increases as well.

The FF decreases after PIII is applied, this effect can be attributed first, to the fact that the resistance between the contacts and the semiconductor surface of the

cell is not improved by PIII and second because PIII acts to increase the bulk contact resistance. Both facts act to increase the series resistance and as a result degrade the FF.

Srv	Voc	VocRel %	Isc	IscRel %	FF	FFRel %	Eff	EffRel %
Experiments								
Untreated Sample 2	0.5682	0	19.48m	0	0.695	0	9.2%	0
PIII Sample2	0.5772	1.5	24.33m	24.8	0.658	-5.6	10.67%	15.97
Untreated Sample 3	0.5794	0	17.69m	0	0.78	0	10.58%	0
PIII Sample3	0.5859	1.1	22.33m	26.22	0.724	-7.73	12.43%	17.48
Simulation								
1e6	0.584	-1.6	9,973E-5	-10.9	68.612	-7.5	8.2	-18
1e5	0.5915	-0.2	1,101E-4	-1.324	73.548	-0.646	9.7349	-2.32
1e4	0.5925	0	1,114E-4	0	74.029	0	9.9735	0
1e3	0.5935	+0.2	1,116E-4	+0.124	74.093	+0.094	9.9986	+0.251
1e2	0.594	+0.26	1,116E-4	+0.133	74.1366	+0.145	10.0012	+0.276
0	0.594	+0.26	1,116E-4	+0.133	74.2623	+0.314	10.0014	+0.278

Table 3.3 *Relation between experimental and simulated results*

Table 3.3 relates experimental and simulated results; the observed tendency is quite similar: both Voc variations are very alike, Isc is the parameter that improves to the highest degree as compared with Voc and FF (the relative amount is lower in the simulation, due to the smaller size of the simulated solar cell). Finally there is a main difference concerning the FF, a parameter that increases when decreasing Srv in the

simulation but increases when applying PIII in the experiments. An Explanation for the different evolution of FF results in simulated and experimental environments has been previously described.

3.5 Summary

A brief theoretical study on the impact of surface recombination velocity on the main solar cell parameters Isc, Voc, FF and Efficiency has been developed. Conclusions on the relation between this factor, the surface defects and the solar cell performance have been stated. A simulated solar cell has been created and tested in order to verify theoretical conclusions. PIII has been applied on the top surface of commercial solar cells, in order to evaluate its passivating and surface modifying characteristics. At last, theoretical, simulated and experimental results were evaluated together and the impact of PIII as a technology of photovoltaic enhancement was examined.

References

[1] Martin A.Green, “Solar Cells Operating Principles, Technology and System Applications.”, p55

[2] Martin A.Green, “Solar Cells Operating Principles, Technology and System Applications.”, p55

[3] Martin A.Green, “Solar Cells Operating Principles, Technology and System Applications.”, p.55

[4] Martin A.Green, “Solar Cells Operating Principles, Technology and System Applications.”, p.81

[5] A. Luque, S. Hegedus, “Handbook of Photovoltaic Science and Engineering.”, 2003, pp 94

[6] A. Luque, S. Hegedus, “Handbook of Photovoltaic Science and Engineering.”, 2003, pp 94

[7] A. Luque, S. Hegedus, “Handbook of Photovoltaic Science and Engineering.”, 2003, pp 94

[8] A. Luque, S. Hegedus, “Handbook of Photovoltaic Science and Engineering.”, 2003, pp 94

[9] J. D. *Bernstein*, S. Qin, C. Chan, and T.-J. King, IEEE Electron Device Letters *16*, pp. *421*-423, Oct. *1995*.

[10] Zhineng Fan, Gang Zhao,Paul K. Chu, Zhonghe Jin, Hoi S. Kwok, and Man Wong, Floating low-temperature radio-frequency plasma oxidation of polycrystalline silicon-germanium, Applied Physics Letters Vol 73, No 3, pp 360-362, July 1998

[11] Jingbao Liu et al: "Formation of Buried Oxide in Siliconusing Separation by

Plasma Implantation of Oxygen", Applied Physics Letters, vol. 67, Nol. 16, Oct. 16, 1995, pp. 2361-2363

[12] X. Lu, S. S. K. Iyer, J. B. Liu, C. M. Hu, N. W. Cheung, J. Min, and P. K. Chu, “Separation by plasma implantation of oxygen to form silicon on insulator,” Appl. Phys. Lett., vol. 70, no. 13, pp. 1748–1750, 1997.

[13] B. Mizuno, I. Nakayama, N. Aoi, M. Kubota and T. Komeda. *Appl. Phys. Lett.* **53** (1988), p. 2059.

[14] S. Qin and C. Chan,”Plasma Doping for Ultra Shallow Junctions” *J. Vac. Sci. Technol. B* 12, 962 (1994).

Chapter 4

Strain Technology in Photovoltaics

4.1 Introduction

The semiconductor manufacturing industry pursues the achievement of Moore's Law adopting a wide range of measures. Scaling down the size of the components chips consist of has been the historical tendency as far as smaller transistors mean both an increase in the switching speed of the devices (smaller gate length is translated into a shorter distance carriers must travel) and also lower manufacturing and production costs. But this traditional optimization tendency encounters (among other drawbacks) a physical limit when gate dielectric limitations are taken into account. Extremely thin gate oxides give rise to undesired leakage currents that diminish the expected efficiency and hence manufacturers are obliged to find alternatives not involving physical shrinking measures.

The use of alternative materials for both gate oxide and transistor channel and the enhancement of carrier mobility through strain are the most popular approaches taken to ensure the accomplishment of Moore's Law.

In this chapter, mechanical strain technology is applied to solar cells in order to benefit from the mobility boosting effects this approach delivers.

Theory referring to strain and its effect on carriers is primarily analyzed, simulation analysis is subsequently carried on with the aid of ISE TCAD software and results obtained are compared with those extracted from commercial solar cell experiments.

4.2 Strain Effect Theoretical Background

Several approaches to manipulate carrier mobility by means of strain exist and each one affects carrier mobility differently because each one has a dissimilar impact on the underlying silicon band structure.

4.2.1 Impact on Semiconductor Bandgap

The band structure of a semiconductor is defined as a complex hybrid energy level model that surrounds every atom in the material's lattice. By applying stress forces on the silicon, its band structure is modified and hence the material properties are affected.

Strain (compressive or tensile) is mainly applied following two schemes. Uniaxial (stress is applied among a single direction) or biaxial (two directions are involved when stress is transferred to the lattice).

Figure 4.1 shows the different band structure of silicon under conditions of no strain, uniaxial strain and biaxial strain.

It is observed that silicon exhibits a 12-fold symmetric surface in three-dimensional space, which is altered after uniaxial or biaxial stress is applied.

Uniaxial stress acts to reduce in plane effective mass (up to 40%) and scattering and hence carriers are able to achieve notably higher mobility enhancement. [2]

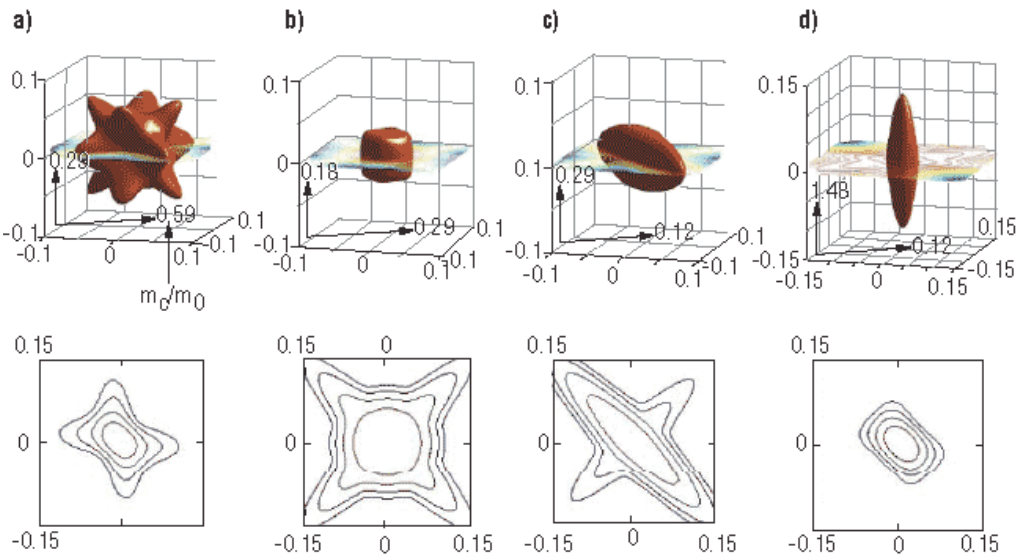

Figure 4.1 *Constant energy surface and energy contours for a)unstressed Si, b) 1GPa biaxial tensile stress, c) 1GPa uniaxial compressive stress on (001) Si, and d) 1GPa uniaxial compressive stress on (110) Si. After [1]*

Under biaxial stress, there is a reduction in scattering deduced from the observation of the effective mass remaining constant, near the value showed by unstrained silicon. Mobility in biaxially strained silicon is attributed to the scattering reduction.

Figure 4.2 shows the conduction and valence band shift arisen in silicon when uniaxially or biaxially strained. Results computed using deformation potential theory[3].

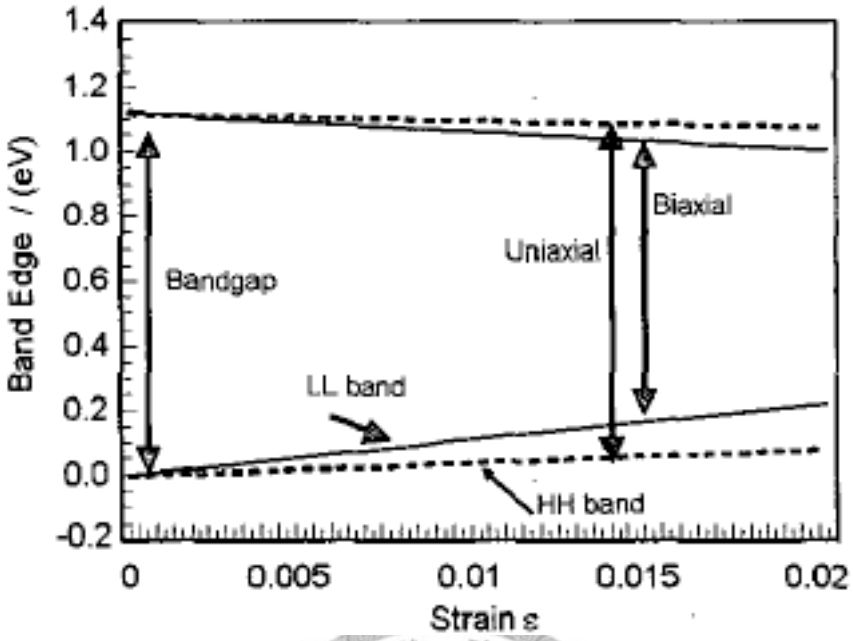

Figure 4.2 *Calculations using deformation potential theory, Si conduction and valence band shift for uniaxial or biaxial stress, after [3].*

4.2.2 Impact on Carrier Mobilities

Figure 4.3 and 4.4 [4] describe the effect biaxial tensile and compressive strain on the <001> direction has on electron and hole mobility respectively. As far as this investigation is concerned, our attention will be mainly focused on lines represented by open circles for both figures, as they represent the out of plane (along the z axis or normal to the plane defined by the silicon layer) mobility, which has the highest impact on solar cell behavior.

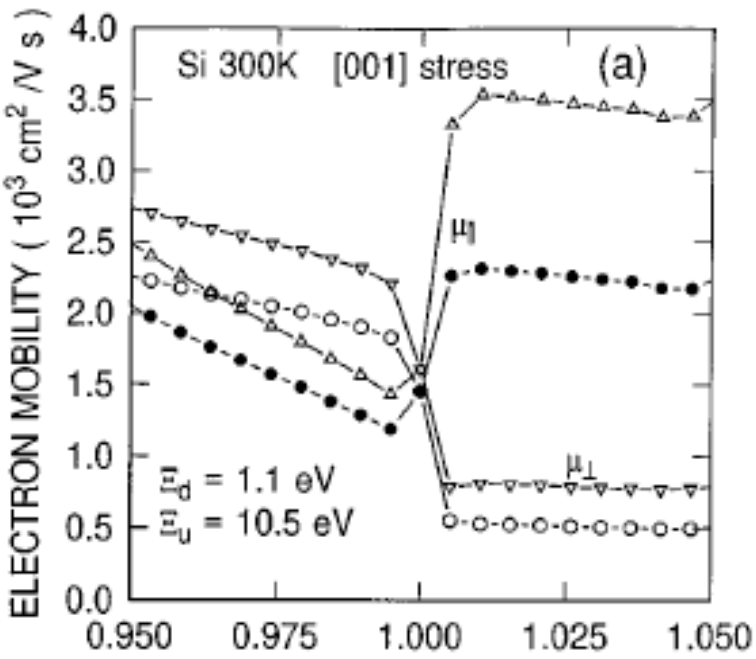

Figure 4.3 *Biaxial tensile and compressive effect on electrons, after [4]*

Electron mobility is enhanced when compressive stress is applied and is reduced when tensile stress is present as it is observed in Figure 4.3.

Figure 4.4 indicates that the hole mobility, on the other side, increases for both compressive and tensile strain.

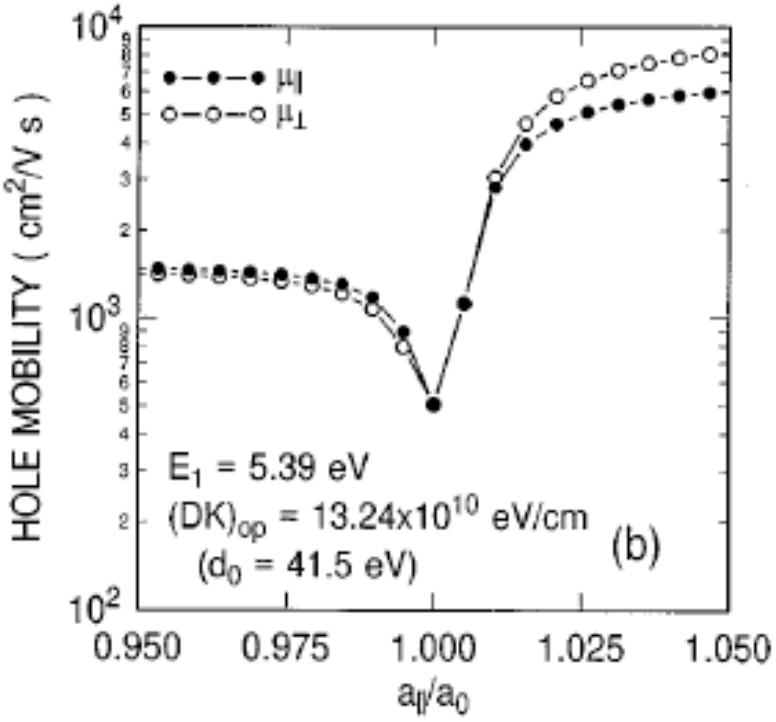

Figure 4.4 *Biaxial tensile and compressive effect on holes, after [4]*

4.2.3 Effect on solar cell behavior

In order to obtain a deeper understanding of the solar cell physical structure when mechanical strain is applied, simulation with the commercial software ANSYS was carried in previous investigations [5]. Figure 4.5 represents the strain distribution on a <001> 230um thick wafer under uniaxial tensile strain along [010] direction. It is observed that the top surface of the solar cell is under tensile stress and the lower part under compressive, with comparable absolute values.

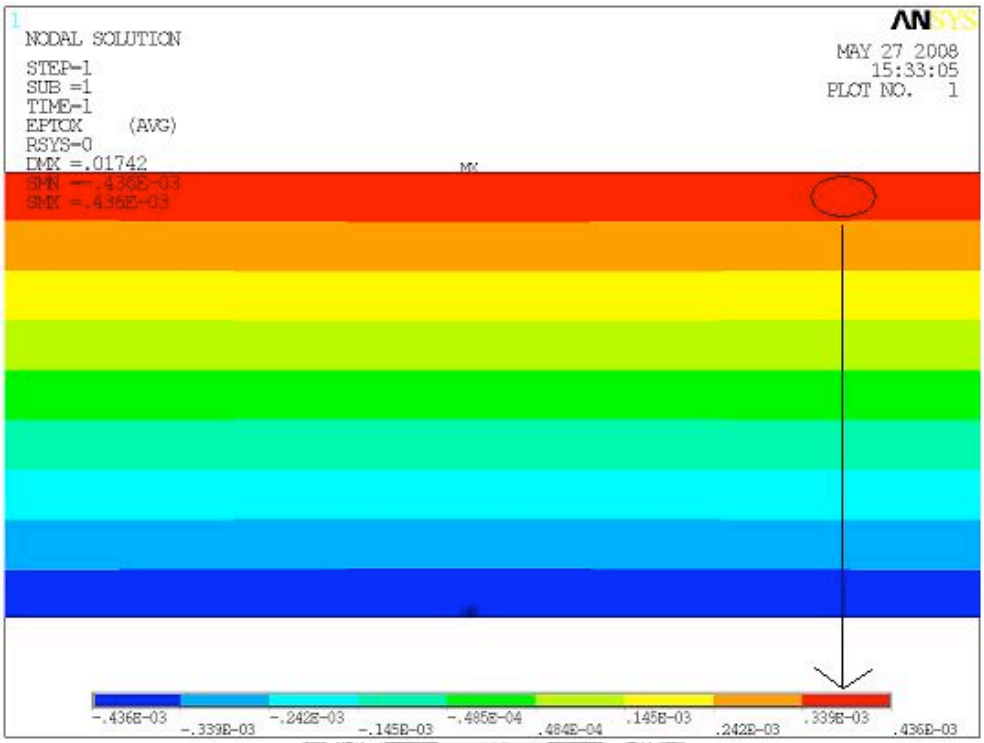

Figure 4.5 *Strain distribution on a silicon wafer under uniaxial stress*

Examining the theoretical considerations developed in previous sections we can predict the variation of the main solar cell parameters when strain is applied:

- Isc is a function of bandgap, the smaller the latter, the larger amount of photons with sufficient energy to generate electron hole pairs that will later contribute to the photocurrent, increasing Isc.

- Voc will decrease as consequence of the bandgap reduction. Smaller bandgap means higher dark current.

- FF will increase. The p type substrate of the solar cell is the most remarkable contributor to the series resistance due its larger size as compared to the emitter region. By applying strain (no matter tensile or compressive) to the solar cell, the hole mobility is increased, provided that holes are the majority carrier in a p type substrate it is deduced that the resistance (series resistance defined by the substrate region) will decrease and the FF will be enhanced.

- Efficiency will be determined by the relative influence each one of the previous factors has on the overall solar cell performance.

4.3 Simulation Outcome

For the purpose of gaining a deeper understanding of the prospects arisen by strain technology on solar cell efficiency enhancement, ISE TCAD commercial software has been utilized in order to simulate a solar cell under reasonable strain conditions. Results obtained are intended to be compared with theoretical and experimental results and hence valuable conclusions can be drawn.

The model defined makes use of the knowledge derived from previous Ansys simulation (figure anterior) which states that the upper half of the solar cell (portion of p type substrate, emitter region and contacts) is under tensile stress and the lower half (p type substrate) is under compressive stress. Biaxial stress simulated absolute values are in the range of 0 to 0.1Gpa so as to approximate to experimentally applied stress values.

Bandgap of silicon under different stress conditions is modified by means of Matlab simulated mathematical models relying on [6] and carrier mobility (electron and hole on p type substrate and emitter regions) is also adapted to the stress environment in which carriers travel, through independent assignment of values based on the paper [4]

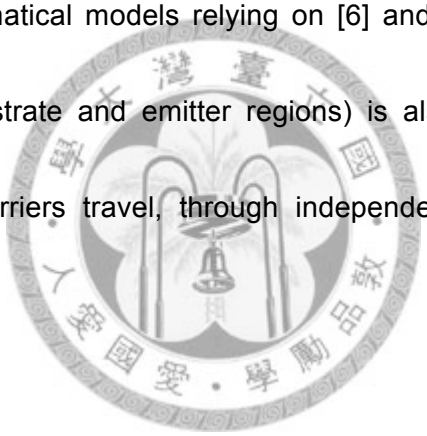

4.3.1 Short Circuit Current (Isc)

Short circuit current experiences an enlargement when strain is increased. From an initial value, with no strain applied, of 3,85E-06 A Isc increases up to 3,94E-06 A under 0.1Gpa biaxial stress. This augment of current represents a 2,085% relative increase over the initial value. Figure 4.6 illustrates the evolution of Isc versus the biaxial strain applied on the solar cell.

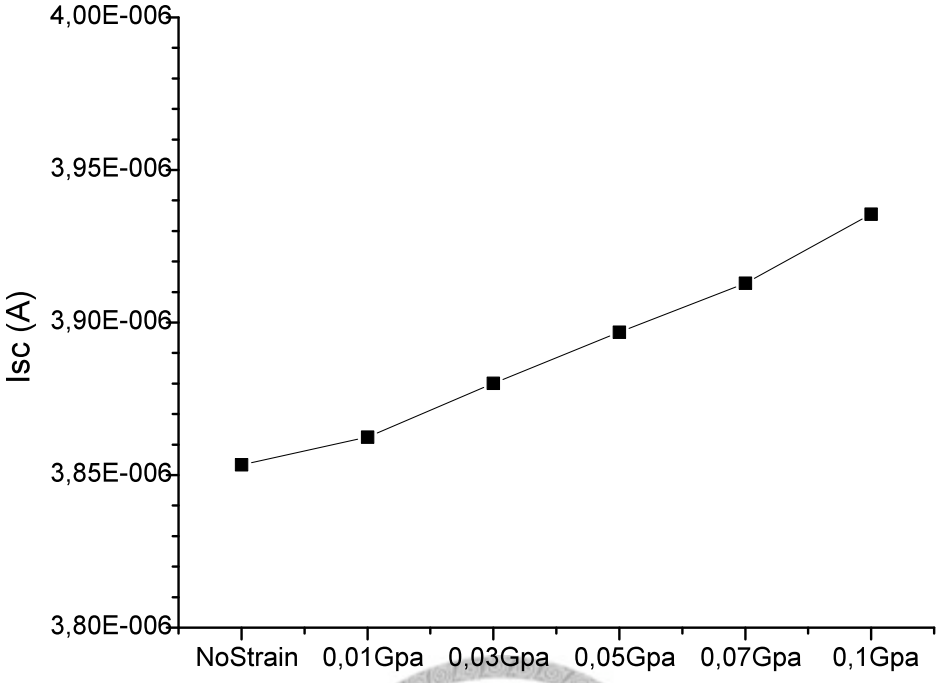

Figure 4.6 *Evolution of Isc versus the biaxial strain applied*

4.3.2 Open Circuit Voltage (Voc)

As it can be observed in figure 4.7, the open circuit voltage exhibits a tendency to decrease when biaxial stress is augmented. Under unstrained conditions Voc equals to 0.504 V and becomes 0.498 under 0.1Gpa biaxial stress. This diminution represents a 1.19% relative deterioration when compared to the original value.

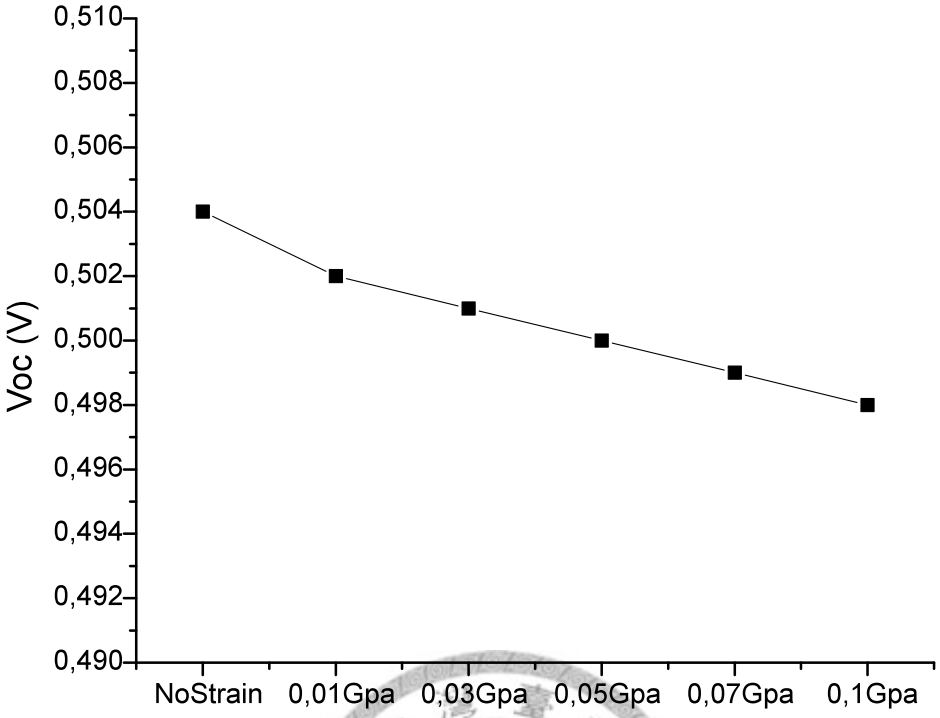

Figure 4.7 *Evolution of Voc versus the biaxial strain applied*

4.3.3 Field Factor (FF)

The Field Factor also experiences a positive evolution when stress is present. From the original 71.5% when the solar cell remains under no stress influence, the FF increases up to 71.89% under 0.1Gpa biaxial condition. The relative percentage this improvement represents is about 0.55%. Figure 4.8 illustrates this effect.

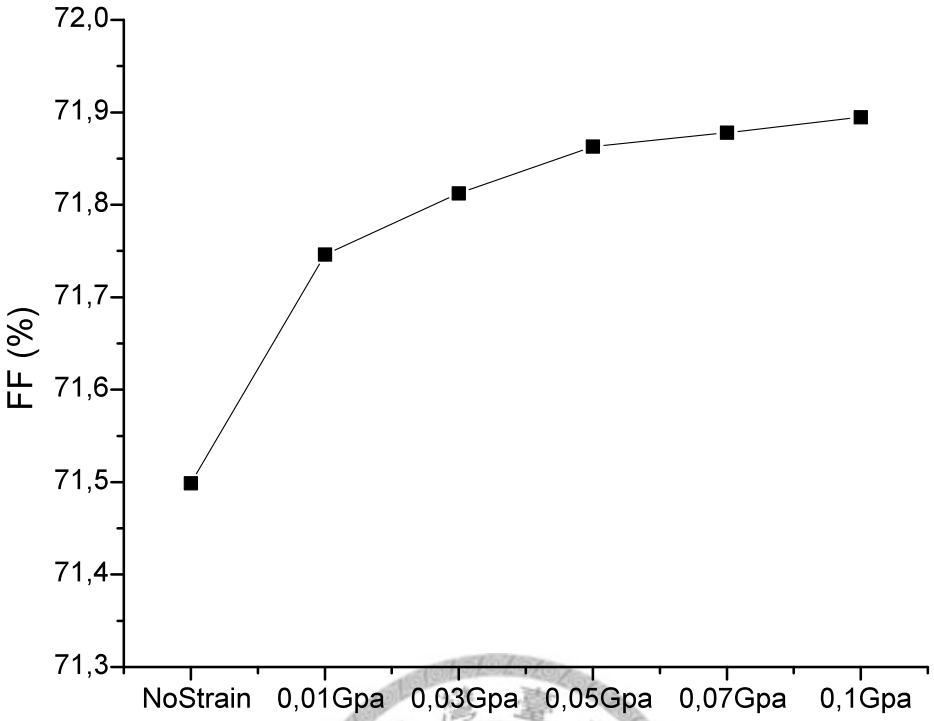

Figure 4.8 *Evolution of FF versus the biaxial strain applied*

4.3.4 Efficiency

Finally, efficiency follows the positive tendency shown by Isc and the FF, an enhancement is observed when biaxial stress is applied. Initially the solar cell efficiency accounts for 13.89% and it is increased up to a 14,09% when 0.1Gpa biaxial stress is applied (Figure 4.9). The relative percentage of enlargement stands for a 1.431%.

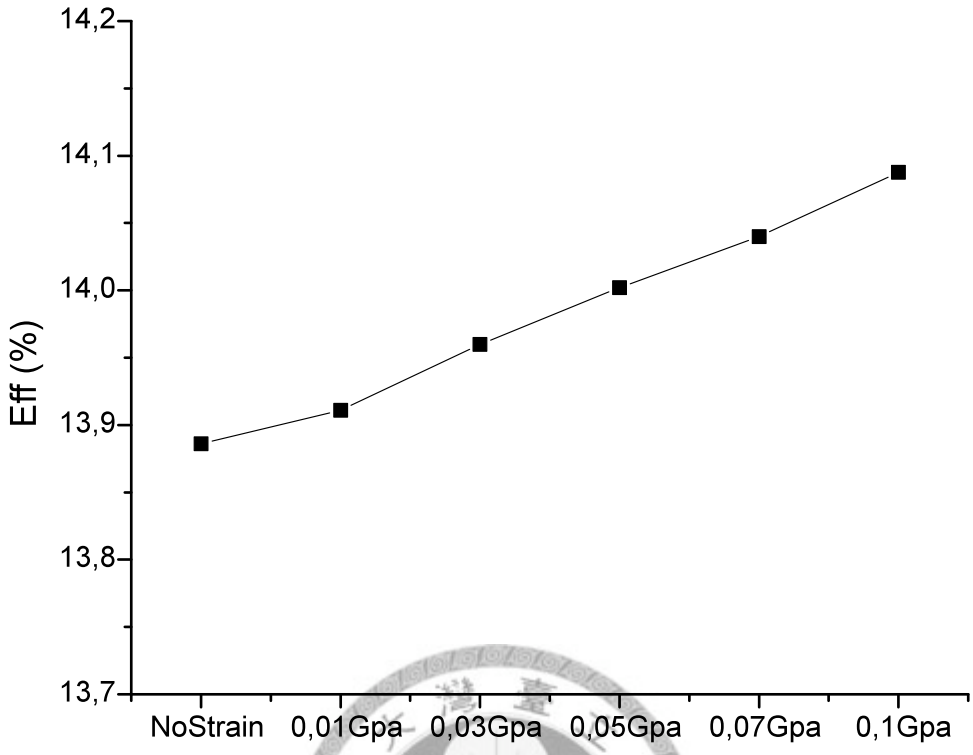

Figure 4.9 *Evolution of Eff versus the biaxial strain applied*

4.4 Discussion

Theoretical prospects indicated that strain influence on bandgap and carrier mobility would effectively boost efficiency.

Results obtained from the simulation are reflected on table 4.1 and table 4.2. It is observed that simulation outputs match theoretical suppositions. A reduction in the bandgap as a consequence of the biaxial stress is translated into a boost of the solar

cell light absorbing capabilities and hence short circuit current magnitude rises. From all the solar cell factors analyzed through the simulation, Isc experiences the highest optimization rate (2,085%).

	Isc	Voc	FF	Eff
No Strain	3,85E-06	0,504	71,4986	13,886
0.01 Gpa	3,86E-06	0,502	71,7461	13,9111
0.03 Gpa	3,88E-06	0,501	71,8124	13,9598
0.05 Gpa	3,90E-06	0,5	71,8629	14,0019
0.07 Gpa	3,91E-06	0,499	71,8779	14,04
0.1 Gpa	3,94E-06	0,498	71,8945	14,0876

Table 4.1 *Evolution of main solar cell parameters (absolute values) with respect to the applied stress.*

Voc is the only parameter that diminishes when the solar cell strain is enlarged, as described in the theory; there is a direct relation between the magnitude of bandgap and the open circuit voltage, as a consequence Voc will lessen when strain is applied.

Hole mobility is increased with biaxial strain, series resistance is reduced and finally a moderate improvement of the field factor is appreciated.

Finally, efficiency is boosted for the reason that the negative effect derived from Voc reduction is compensated and overcome with the combined enhancement of Isc and FF.

	Isc	Voc	FF	Eff
No Strain	3,85E-06	0,504	71,4986	13,886
0.01 Gpa	0,232%	-0,396%	0,344%	0,180%
0.03 Gpa	0,687%	-0,595%	0,436%	0,528%
0.05 Gpa	1,114%	-0,793%	0,506%	0,827%
0.07 Gpa	1,519%	-0,992%	0,527%	1,096%
0.1 Gpa	2,085%	-1,190%	0,550%	1,431%

Table 4.2 *Evolution of main solar cell parameters (relative values) with respect to the applied stress.*

4.5 Summary

A superficial theoretical examination on the influence of strain on the silicon structure was elaborated and the effect of biaxial stress on semiconductor bandgap, and carrier mobility was analyzed. Impact of these modifications on the solar cell behavior was initially theorized and later contrasted with results obtained from solar cell simulations carried with the aid of ISE Tcad software. Simulated solar cells respond positively to biaxial strain and consequently application of stress on solar cells stands as a promising technology that can successfully boost efficiency.

References

[1] S.E. Thompson, G. Sun, K. Wu, J. Lim, and T. Nishida

"Key Differences For Process-induced Uniaxial vs. Substrate- induced Biaxial Stressed Si and Ge Channel MOSFETs"

[2] S.E. Thompson, et al.,

"Key Differences for Process-induced Uniaxial vs. Substrate-induced Biaxial Stressed Si and Ge Channel MOSFETs,"

[3] S.E. Thompson, et al.

"Future of Strained Si/Semiconductors in Nanoscale MOSFETs,"

[4] M. V. Fischettia and S. E. Laux

"Band structure, deformation potentials, and carrier mobility in strained Si, Ge, and SiGe alloys."

[5] Tsai, Jyun-Jhe (Master Thesis)

"Characterization of Crystalline Silicon-Based P-N Junction Solar Cells and Fabrication of Germanium MIS Thin Film Solar Cells"

[6] Chris G. Van de Walle

"Band Lineups and Deformation Potentials in the Model-Solid Theory"

Chapter 5

Summary and Future Work

5.1 Summary

In this thesis efficiency boosting techniques for wafer solar cells have been developed in order to provide performance enhancement approaches that may benefit the emerging photovoltaic technologies.

In chapter 2, MIS devices were theoretically analyzed under dark current and illumination conditions. Simulations showed similar results to those theoretically predicted. MIS solar cells were fabricated, their IV curves obtained, and the results compared with those from simulated devices. Al/SiO2/ptype devices showed similar qualitatively results to those obtained from simulation while extremely negative results acquired with ITO/SiO2/nType substrate discard the utilization of transparent conductive oxides as promising contact materials for MIS solar cells.

In chapter 3, a brief theoretical study on the impact of surface recombination velocity on the main solar cell parameters Isc, Voc, FF and Efficiency has been developed. Conclusions on the relation between this factor, the surface defects and the solar cell performance have been stated. A simulated solar cell has been created and tested in order to verify theoretical conclusions. PIII has been applied on the top

surface of commercial solar cells, in order to evaluate its passivating and surface modifying characteristics. At last, theoretical, simulated and experimental results were evaluated together and the impact of PIII as a technology of photovoltaic enhancement was examined.

Finally in chapter 4, a superficial theoretical examination on the influence of strain on the silicon structure was elaborated and the effect of biaxial stress on semiconductor bandgap, and carrier mobility was analyzed. Impact of these modifications on the solar cell behavior was initially theorized and later contrasted with results obtained from solar cell simulations carried with the aid of ISE Tcad software. Simulated solar cells respond positively to biaxial strain and consequently application of stress on solar cells stands as a promising technology that can successfully boost efficiency.

5.2 Future Work

As far as the second chapter is concerned, it has been shown how complicated the relation between material workfunction and solar cell behavior is, and the low performance MIS devices with alternative front contacts (ITO) exhibit, hence the recommended future work should be focused on the third and forth chapters.

On the third chapter experiments have been carried on small pieces obtained

from 6 inch polycrystalline solar cells, recommended work include carrying experiments on big solar cells, and further analysis on how the FF factor is affected after solar cells are PIII treated.

The fourth chapter analyses strain effect on solar cells with the aid of simulation software, in order to verify these results and later improve solar cell performance experiments on physical solar cells should be carried. With this aim, our laboratory has developed the appropriated machinery (Figure 5.1) and experiments are already being performed. Results should be reported elsewhere in a brief period of time

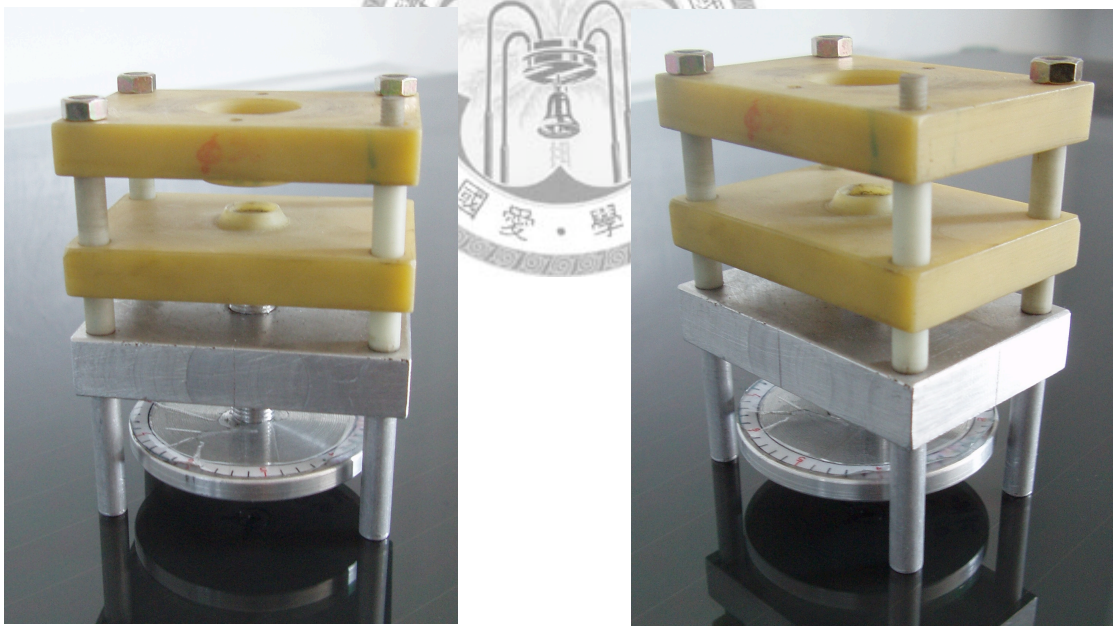

Figure 5.1 *Mechanical strain induction devices engineered in our laboratory*